
Interactions of surface and deep anticyclonic eddies in the Bay of Biscay

Xavier Carton^{a,*}, Bernard Le Cann^a, Alain Serpette^b, Jesus Dubert^c

^a Laboratoire de Physique des Océans, UMR6523 UBO-CNRS-IRD-IFREMER, Université de Bretagne Occidentale, Brest, France

^b Centre d'Hydrographie, d'Océanographie et de Météorologie Militaire, Service Hydrographique et Océanographique de la Marine, Brest, France

^c Departamento de Física & CESAM, Universidade de Aveiro, 3810-193 Aveiro, Portugal

*: Corresponding author : Xavier Carton, Tel.: + 33 298016219 ; email address : xcarton@univ-brest.fr

Abstract:

In 1990, satellite observations revealed that an anticyclonic surface eddy (a SWODDY, for Slope Water Oceanic eDDY) followed a cycloidal trajectory north of the Iberian coast in the Bay of Biscay. To understand the mechanisms underlying such a trajectory, we study the evolution of an idealized surface eddy in a two-layer flat-bottom quasi-geostrophic model. The effect of several processes is studied, notably the presence of deep anticyclonic vorticity. This deep vorticity may result either from the tilting of the swoddy itself, or from the presence of an anticyclonic eddy of different origins, such as a meddy (Mediterranean Water EDDY). We also study the influence of a zonal coast south of the swoddy, via the “mirror effect”.

Firstly, a point-vortex model is used on the f -plane. When the surface and deep vortices lie much farther away from the coast than from each other, their motion is close to the addition of a mutually induced rotation and of a quasi-uniform zonal drift induced by the mirror vortices. The sensitivity of the rotation and translation characteristics to vortex position, strength, thickness and to a surrounding flow, are investigated. Such a surface-deep vortex interaction can reasonably well represent the observed motions of the swoddy, if the deep vortex is far enough from the surface one, and if they have comparable strengths.

Then, a numerical code of the two-layer quasi-geostrophic equations is used to model finite-area vortices, again on the f -plane. Vertical alignment of the surface and deep vortices or vortex pairing with the mirror image, are not observed. Vortex splitting due to mutual shearing effects occurs only for vortices with very different strengths. Vortex trajectories similar to the ones observed are reproduced by the model for equal strength vortices.

Complementary data, from the CONGAS experiments in 2004–2007, and from the ARGO profiling float database, are used to show that meddies (or at least coherent salinity anomalies at 1000 m depth) can originate from the continental slope near 45°N, 8°W and move regularly northeastward toward the region of swoddy generation and drift. These data also show that meddy–swoddy (“deep vortex–surface vortex”) encounters may occur in the southeastern Bay of Biscay.

Keywords: Bay of Biscay ; Anticyclonic eddies ; Swoddy ; Meddy ; Point vortex dynamics ; Trajectory; Quasi-geostrophic model ; In-situ observations

1 Introduction

A poleward slope current, forced by wind stress and by large-scale density gradients, flows along the Western and Northern coast of the Iberian Peninsula in winter (Pingree and Le Cann, 1989; Frouin et al., 1990; Haynes and Barton, 1990; Garcia-Soto et al., 2002). This current exhibits a major interannual variability, and when strong enough, penetrates in the Bay of Biscay up to the Cape Ferret Canyon, which indents the continental slope of Aquitaine near 45°N , $2^{\circ}30'\text{W}$ (Pingree and Le Cann, 1990). Though the mean currents are weak (on the order of 5-10 cm/s), strong currents in excess of 100 cm/s have been recorded locally (Le Cann and Serpette, 2009). This current has a baroclinic character: the mean flow direction near 500m depth is opposite to that of the mean surface current (Pingree and Le Cann, 1989). Satellite observations of sea surface temperature show that Cape Ortegal and the Cape Ferret Canyon are sites where this poleward current may be destabilized. This destabilization can lead to the formation of surface-intensified eddies, which trap warm water and are anticyclonic; these eddies were called SWODDIES for Slope Water Oceanic eDDIES (Pingree and Le Cann, 1992a,b). In particular, in 1990, three SWODDIES were observed, two of them originating from the Cape Ferret Canyon, F90a and F90b, and one formed near Cape Ortegal, O90. In this paper, we will study F90a in more detail (see its trajectory on figure 1).

Hydrographic measurements of F90a (Pingree and Le Cann, 1992a) indicate that, based on isotherm 12.5°C displacements, its hydrological radius is about 50 km whereas maximum azimuthal velocity (equal to 30 cm/s) is obtained at a radius of about 30km. The 12.5°C isotherm (or the $\sigma = 27.0 \text{ kg/m}^3$ isopycnal) deepens from 100 m depth in the eddy periphery to about 300 m depth at its core, and a 1°C temperature anomaly, between the eddy core and its surroundings, is clearly observed near 200 m depth. Though the eddy is stronger in the upper 350 m of the ocean, its dynamical and hydrographical signatures extend down to at least 1800 m depth.

The trajectory of F90a is remarkable because it is cycloidal with North-South extension of about 120 km and a zonal periodicity of about 320 km at speeds around 2 cm/s (figure 1). On average, this trajectory is mostly westward. The question thus arises of the physical mechanisms which underlie this particular trajectory; is it due to:

- the swoddy baroclinicity (see also Dubert, 1993),
- the presence of another eddy,
- the influence of the coast (via "mirror vortices"),
- or advection by the large-scale circulation (which is meridionally sheared, see Koutsikopoulos and Le Cann, 1996).

Note that other mechanisms such as beta-effect (Bertrand and Carton, 1993), or wind-induced propagation (Morel and Thomas, 2009) are not considered here.

In fact, cycloidal features have already been observed in trajectories of other oceanic eddies, e.g. for meddy "Ulla" observed to recirculate near the Charcot seamounts (Paillet et al., 1999; 2002), for meddy "Christine" which interacted with the southern Horseshoe seamounts (Carton et al., 2002) and for other eddies (Reverdin et al., 2009). But F90a drifts over the abyssal plain and therefore no prominent topographic feature can explain its particular trajectory, contrary to meddy "Ulla" or to meddy "Christine", for example.

Here, we address this problem from the point of view of "process studies". Our aim is

to determine, in a very simple model, which physical mechanism can induce this specific trajectory. We idealize the swoddy as a baroclinic, pointwise or finite area, vortex in a two-layer flat bottom quasi-geostrophic model. The coast of Spain is simplified into a zonal southern boundary of the model. Wind-stress and thermohaline forcing are discarded, to account only for the nonlinear mesoscale dynamics.

Firstly, we will provide estimates of drift velocity for a point vortex. Secondly, we will analyze the influence of the effects mentioned above, with a numerical point vortex model on the f-plane. Thirdly, we will use a numerical model for finite-area vortices to explore the influence of finite vortex size; we will provide a possible explanation of the observed drift of swoddy F90a. Finally, we will present in-situ data which give support to the realism of this explanation.

2 The quasi-geostrophic model and physical configuration

The Rossby and Burger numbers of swoddy F90a, based on its maximum azimuthal velocity U , radius of maximum velocity L and thickness H are $Ro = U/fL = 0.1$, $Bu = (NH/fL)^2 = 0.3$. Here f is the Coriolis parameter and N the Brunt Vaisala frequency. The relative amplitude of vertical deviations of isopycnal surfaces is $\Delta h/H \approx Ro/Bu$ for a vortex in cyclogeostrophic balance (see for instance, Carton, 2001). A quasi-geostrophic model can be used to describe the swoddy, but since $\Delta h/H$ is not very small, further studies should be undertaken with a shallow-water primitive-equation model to investigate the influence of cyclone- anticyclone parity bias. We choose a two-layer configuration of the quasi-geostrophic model, which is the simplest possible to accommodate the baroclinic character of the swoddy, or the possible existence of a deep eddy, the deeper ocean being considered at rest.

The quasi-geostrophic dynamics of unforced, non dissipative motions, are characterized by the conservation of their potential vorticity¹ q_j (with upper, lower layer indices $j = 1, 2$). Here, we write this conservation on the f-plane:

$$\frac{dq_j}{dt} = 0,$$

with the upper layer potential vorticity

$$q_1 = \nabla^2\psi_1 + F_1(\psi_2 - \psi_1) + f_0$$

and the lower layer potential vorticity

$$q_2 = \nabla^2\psi_2 + F_2(\psi_1 - \psi_2) + f_0.$$

The streamfunction in layer j is $\psi_j(x, y, t)$ and f_0 is the Coriolis parameter. The layer coupling coefficients are

$$F_1 = \frac{f_0^2}{g'H_1}, \quad F_2 = \frac{f_0^2}{g'H_2}$$

¹Quasi-geostrophic potential vorticity is the shallow-water potential vorticity anomaly with respect to a state of rest, multiplied by the layer thickness, in the limit of small Rossby number and of order unity Burger number

where, H_j are the layer thicknesses at rest, and, using ρ_0 as an average density, the reduced gravity is defined by $g' = g(\rho_2 - \rho_1)/\rho_0$. We also note $h_j = H_j/H$ the fractional depth of layer j (with $H = H_1 + H_2$).

In the two-layer model, the barotropic and baroclinic modes are defined by

$$\psi_{bt} = h_1\psi_1 + h_2\psi_2, \quad \psi_{bc} = \psi_1 - \psi_2$$

Potential vorticity is related to streamfunction in each mode via

$$q_{bt} = \nabla^2\psi_{bt}, \quad q_{bc} = \nabla^2\psi_{bc} - \psi_{bc}/R_d^2$$

where R_d is the internal deformation radius $R_d = \sqrt{g'H_1H_2/H}/f_0$ (and we note $\gamma = 1/R_d$).

3 The analytical and numerical results from the point vortex model

In this section, we use a point vortex approximation of the swoddy to describe its cycloidal trajectory on the f-plane. Beta-plane models exist for point vortices (see Zabusky and McWilliams, 1982), but the influence of beta effect on the evolution of two vortices would constitute a separate study.

Firstly, we will exhibit analytical solutions for simple trajectories; secondly, we will simulate the evolution of baroclinic vortices in a numerical code for point vortices.

The model configuration is sketched on figure 2. The flow domain is $x \in [-L_x/2, L_x/2]$ and $y \geq 0$. The coast is located at $y = 0$. We consider two point vortices ("a" and "b"), and their mirror images across the coast. Point vortex "a" is located in the upper layer and has a charge² $Q_a\delta(x_a, y_a)$, where δ is the Dirac distribution, and Q_a the amplitude of the charge. Hereafter, we will call it the surface vortex. Point vortex "b" is located in the lower layer and has a charge $Q_b\delta(x_b, y_b)$. Hereafter, we will call it the deep vortex. Their mirror images have charges $-Q_a\delta(x_a, -y_a)$ and $-Q_b\delta(x_b, -y_b)$. Note that if "a" and "b" are vertically aligned, or only slightly separated horizontally, they can be considered as the two parts of a single eddy (the swoddy), whereas if they initially lie several deformation radii apart, they must naturally be considered as distinct eddies (e.g. the swoddy and a deep eddy). More generally, the association of opposite signed vortices in two layers is called a heton and that of like-signed vortices, an anti-heton (Hogg and Stommel, 1985).

3.1 Equations of motion for point vortices in the presence of the coast

Using the layerwise Green's functions

$$G_{11}(r) = \frac{h_1}{2\pi}\ln(r) - \frac{h_2}{2\pi}K_0(\gamma r), \quad G_{12}(r) = \frac{h_2}{2\pi}\ln(r) + \frac{h_2}{2\pi}K_0(\gamma r)$$

²The charge is the area integral of potential vorticity, analogous to a circulation

$$G_{21}(r) = \frac{h_1}{2\pi} \ln(r) + \frac{h_1}{2\pi} K_0(\gamma r), \quad G_{22}(r) = \frac{h_2}{2\pi} \ln(r) - \frac{h_1}{2\pi} K_0(\gamma r)$$

with K_0 the modified Bessel function of second kind of zero order, and their derivatives with respect to r that we call G'_{ij} , the velocities of vortices "a" and "b" are

$$\begin{aligned} u_a &= \frac{2y_a}{r_{a-a}} Q_a G'_{11}(r_{a-a}) + \frac{y_a + y_b}{r_{a-b}} Q_b G'_{12}(r_{a-b}) - \frac{y_a - y_b}{r_{ab}} Q_b G'_{12}(r_{ab}) \\ v_a &= -\frac{x_a - x_b}{r_{a-b}} Q_b G'_{12}(r_{a-b}) + \frac{x_a - x_b}{r_{ab}} Q_b G'_{12}(r_{ab}) \\ u_b &= \frac{2y_b}{r_{b-b}} Q_b G'_{22}(r_{b-b}) + \frac{y_a + y_b}{r_{b-a}} Q_a G'_{21}(r_{b-a}) - \frac{y_b - y_a}{r_{ba}} Q_a G'_{21}(r_{ba}) \\ v_b &= -\frac{x_b - x_a}{r_{b-a}} Q_a G'_{21}(r_{b-a}) + \frac{x_b - x_a}{r_{ab}} Q_a G'_{21}(r_{ab}) \end{aligned} \quad (1)$$

with the distances between the point vortices and/or their images:

$$r_{ab}^2 = r_{ba}^2 = (x_a - x_b)^2 + (y_a - y_b)^2, \quad r_{a-b}^2 = r_{b-a}^2 = (x_a - x_b)^2 + (y_a + y_b)^2, \quad r_{a-a} = 2y_a, \quad r_{b-b} = 2y_b$$

We set $2y_c = y_a + y_b$, $\xi = x_b - x_a$, $\eta = y_b - y_a$, $d^2 = \xi^2 + \eta^2$.

In these equations, we can identify many dimensionless physical parameters: Q_b/Q_a , $(2y_c)/R_d$ at $t = 0$, d/R_d , h_1/h_2 and the initial orientation of the vortex pair $\phi = \text{atan}(\eta/\xi)$ at $t = 0$. If a uniform mean flow U is added, the corresponding parameter is Ud/Q_a . Finally, a large-scale velocity strain and shear of strength s can be added; the associated dimensionless parameter is s/Q_a .

3.2 Simplified equations of motion for point vortices far away from the coast

Simple analytical solutions can be found when the vortices lie far away from the coast and farther from each other than one internal radius of deformation ($2y_c \gg d \gg R_d$). In this case, the equations are readily simplified into

$$\begin{aligned} u_a &\equiv \frac{h_1 Q_a + h_2 Q_b}{4\pi y_c} + \frac{\eta}{d} Q_b G'_{12}(d) \\ v_a &\equiv -\frac{\xi}{d} Q_b G'_{12}(d) \\ u_b &\equiv \frac{h_1 Q_a + h_2 Q_b}{4\pi y_c} - \frac{\eta}{d} Q_a G'_{21}(d) \\ v_b &\equiv \frac{\xi}{d} Q_a G'_{21}(d) \end{aligned} \quad (2)$$

In these equations, the last term represents the mutual interaction of vortices "a" and "b". Depending on the signs of Q_a and of Q_b , this interaction will lead to a translation or to rotation of the two vortices.

The first term in the zonal velocity is the mirror effect. At large distance from the coast, the

zonal velocity due to the mirror effect is the same for the two vortices: $(h_1Q_a + h_2Q_b)/(4\pi y_c)$.

In these equations, the physical parameters h_1, h_2, Q_a, Q_b appear only as two products h_1Q_a and h_2Q_b which are the depth integrated strengths of the point vortices. Whatever the ratio of these two products (except for -1), one can define a center of rotation for the two vortices via $x_c = [h_1Q_ax_a + h_2Q_bx_b]/[h_1Q_a + h_2Q_b]$ and $y_c = [h_1Q_ay_a + h_2Q_by_b]/[h_1Q_a + h_2Q_b]$. It is straightforward to show that $v_c = dy_c/dt = 0$ so that this center of rotation translates zonally with uniform velocity $u_c = [h_1Q_a + h_2Q_b]/(4\pi y_c)$. Thus the point vortex motion is the addition of a rotation and of a uniform zonal translation.

3.3 Estimating the physical parameters of the point vortex system from observations

Under these conditions, we can estimate the zonal and meridional wavelengths of the motion and its period. The meridional wavelength is then equal to the initial distance between the two vortices since the variations in meridional motion due to the mirror effects have been neglected. We have $\lambda_y = d$. Equations (2) provide the rotation period of the two vortices, which is (in the case of equal strength vortices and equal layer thickness)

$$T = 2\pi/\Omega \approx 2\pi/(h_2Q_b/\pi d^2) = 2\pi^2 d^2/h_2Q_b$$

when neglecting the baroclinic component. The mean average velocity is (again approximately)

$$\bar{U} = (h_1Q_a + h_2Q_b)/(4\pi y_c)$$

so that the 'zonal wavelength' (average zonal displacement of the vortex pair during a period) is

$$\lambda_x = \bar{U}T = \frac{\pi d^2}{2y_c} \left(1 + \frac{h_1Q_a}{h_2Q_b}\right)$$

Thus, since $\lambda_y = d$, we obtain $d \approx 120$ km. Then, *if we assume that the vortices have equal depth-integrated strengths*, we have $\lambda_x = \frac{\pi d^2}{y_c}$. With $\lambda_x \approx 320$ km, this leads to $y_c \approx 140$ km. Conversely, this value of y_c (140 km) is about the distance from the mid latitude of swoddy F90a trajectory and the 1000 m isobath. We know (from data) that $R_d \approx 30$ km in the deep part of the Bay of Biscay. Going back to the initial assumptions for our simplified model ($2y_c \gg d \gg R_d$), we note that the second part of this inequality is better verified than the first one. Thus, one may expect differences between the simplified and the complete model results, in terms of the influence of mirror-image vortices due to the coast.

Figure 1 indicates that $T \approx 5 - 6$ months (for the first and second loops respectively). With this, we can compute the swoddy potential vorticity (and that of its hypothesized deep companion vortex). Assuming that both vortex radii are equal to the first internal deformation radius, $R = R_d$, that $h_1 = h_2$, and that $q_a = q_b$ (with $Q_a = q_a\pi R_d^2$), we have $q_a = q_b \approx -1.5 \cdot 10^{-5} \text{ s}^{-1}$. This estimate is reasonable, considering that the maximum azimuthal velocity of the swoddy is about 0.3 m/s at a radius of 30 km. Concerning the deep eddy, this estimate would be reasonable, though perhaps a bit weak, for a meddy in the Bay of Biscay (see Paillet et al., 2002). Conversely, when $q_a = q_b \approx -2 \cdot 10^{-5} \text{ s}^{-1} = 2U_{max}/R$, we have $T \approx 4 - 5$ months, again close to the observations.

3.4 Numerical simulations

Numerical simulations of point vortex evolutions are performed on the f-plane. A fourth order Runge-Kutta scheme is used to integrate equations (1) in time. We immediately eliminate the case where $Q_b = 0$ for which the vortex does not drift in the absence of the coast, and drifts steadily zonally in its presence. We also eliminate the case where the vortices are initially vertically aligned, leading to a zonal translation. Finally, we do not consider opposite-signed vortices which do not correspond to the observed situation.

Therefore, the translation of the vortex will be due to the mirror effect of the coast.

Dimensional values will be used in the plots for direct comparison with the observations.

3.4.1 The reference simulation

The purpose of this first simulation is to evaluate if the observed swoddy trajectory can be reasonably well reproduced by the very simple point vortex model, using the physical parameters that we calculated above. We set $y_c/R_d = 4.67$, $d/R_d = 4$ and we assume first that the two vortices have the same depth-integrated strength $(h_1Q_a)/(h_2Q_b) = 1$. Figure 3a displays the surface and deep vortex trajectories. The surface vortex path is similar to that in observations (see figure 1).

We note (figure not shown) that the distance between the two vortices in the numerical model has a nearly sinusoidal variation with time; a maximum (resp. minimum) distance between them occurs when the two vortices are parallel (resp. perpendicular) to the coast. When any of the vortices comes close to the southern coast, it feels a stronger influence of the mirror vortices. Thus, it comes closer to its companion vortex, its rotation accelerates, and it moves away from the coast; then, the influence of the mirror vortices decreases. The opposite occurs when the vortices are parallel to the coast.

We can compute the zonal and meridional wavelengths and the total duration of the two loops in the model, and compare them to observations. The zonal wavelength in the numerical model is 295 km instead of 320 for the observations, the meridional wavelength is 103 km instead of 120 km, and the total duration of the two loops in the numerical experiment is one year to be compared with eleven months in the observations. Despite the simplicity of our model, the relative error is thus about 10 %.

Sensitivity experiments will now evaluate how these results vary when the initial positions, or the vortex strengths, are changed, or when surrounding currents are added.

3.4.2 Influence of the distance from the coast

Our first analysis of the numerical model results pertains to the accuracy of the simplified equations (2). This accuracy will depend at first order on $2y_c/d$. For this first series of sensitivity experiments, we set $(h_1Q_a)/(h_2Q_b) = 1$, $d/R_d = 4$. The two vortices are initially aligned zonally. We vary y_c/R_d from 1 to 10.

The theoretical estimate of the zonal wavenumber can be compared to the value of λ_x measured in numerical experiments (see figure 3b). Despite our approximations, a good agreement exists between the two values (with relative errors smaller than, or equal to 15%, for $y_c/R_d \geq 4$). For $y_c/R_d = 2$, the relative error reaches 50 %. Indeed, in this case, both vortices come periodically close to the coast, so that the trajectory is not the addition of a uniform translation and of a circular motion.

We also plot the meridional displacement of the vortices, λ_y , versus y_c , on figure 3c, for $d/R_d = 4$. Again, at large distances from the coast, this "meridional wavelength" is approximately equal to the vortex separation. But now, the effect of the mirror vortices is to repel the real vortices meridionally, so that λ_y decreases with y_c (in simple words, the trajectories flatten against the wall).

Both figures 3b and 3c indicate that the asymptotic equations (2) become less accurate when $2y_c/d \approx 1$ or when $y_c/R_d \approx 1$.

3.4.3 Influence of the vortex separation and orientation

To start again from the asymptotic dynamics (equations (2)), we set $y_c/R_d = 4.67$ (as initial position), and we increase d/R_d from 1 to 7. The values of λ_x and of λ_y are plotted versus d on figures 4a and 4b. For $d > y_c$, the relation $\lambda_x(d) \approx d^{4/3}$ was found via a logarithmic plot (not shown here), but no simple power law could be established for $\lambda_y(d)$.

The initial orientation of the vortex pair has a modest influence on vortex trajectories far away from the coast. For instance, for $y_c/R_d = 6$ and $d/R_d = 4$, the zonal and meridional wavelengths are 241 and 81 km if the pair is oriented zonally initially, and 300 and 120 km if it is oriented meridionally. The effect of the orientation will be more sensitive if the pair is closer to the coast initially, because it will strongly modify the mirror vortex influence. The experiment with $y_c/R_d = 4$ and $d/R_d = 4$ leads to $(\lambda_x; \lambda_y) = (332; 96)$ km for a zonal vortex pair, and $(580; 120)$ km for a meridional pair.

For an application to the Bay of Biscay, it is less likely that the vortex pair may have been in a meridional orientation initially, because the deep vortex would have lain very close to the Spanish continental slope.

3.4.4 Influence of the vertical asymmetry of the vortex or of the layers

Here we investigate the effect of having $Q_a/Q_b \neq 1$ or $h_1/h_2 \neq 1$. In the complete point vortex model (2), both ratios can act independently. In the simplified equations (3) only the ratio $(h_1Q_a)/(h_2Q_b)$ intervenes.

It can be simply anticipated that decreasing Q_a/Q_b from unity with $h_1/h_2 = 1$ or conversely (decreasing h_1/h_2 while keeping $Q_a/Q_b = 1$) will lead to smaller loops for the deep vortex than for the surface one, because the depth integrated strength of the deep vortex will be larger. This is clearly seen in figures 5a-5b where we doubled the strength of the deep vortex: the meridional wavelength of the upper (resp. lower) layer loops has increased (resp. decreased) with respect to the reference experiment. Several numerical experiments, varying $(h_1Q_a)/(h_2Q_b)$ from 1 to 2.5, show that the zonal wavelength λ_x is smaller in both layers for unequal strength vortices; but the ratio of these layerwise zonal wavelengths $\lambda_{x1}/\lambda_{x2}$ remains close to unity in that range of $(h_1Q_a)/(h_2Q_b)$. On the contrary, the ratio of layerwise meridional wavelengths $\lambda_{y1}/\lambda_{y2}$ scales as $(h_2Q_b)/(h_1Q_a)$ (figure not shown).

Also, when the deep vortex is stronger than in the reference experiment, the vortices rotate faster than in the reference case.

One can also ask if a vertically asymmetric vortex doublet could lead to surface vortex trajectories closer to observations than in the reference case. The modeled surface vortex trajectory was found closest to the observations when $y_c/R_d = 4.67$, $(h_1Q_a)/(h_2Q_b) = 1.5$ and $d/R_d = 4.5$ (among many simulations performed). We show the vortex trajectories in

this case on figure 5c. The zonal wavelength is now about 350 km and the meridional one 130 km. But the loops of the surface vortex are more opened than in the reference experiment and than in the observations. Now, again, other physical effects exist in the ocean which are not taken into account here and which may explain the difference in the shape of trajectories. Therefore we conclude that both equal strength vortices, or vortices with slightly unequal strengths, but within a realistic ratio, could lead to trajectories similar to that observed in the Bay of Biscay.

3.4.5 Influence of a non-uniform, large-scale flow

It is known that an anticyclonic circulation exists at large scale over the abyssal plain of the Bay of Biscay (Pingree, 1993; Koutsikopoulos and Le Cann, 1996; Serpette et al., 2006). Here, we idealize this circulation by simple large-scale flows. We do not study the case of a uniform zonal flow which simply adds a constant advection to the vortex pair. We will successively consider the cases of a shear flow and of a strain flow.

For a shear flow, we use the form $U = s(y - L_y)$, where $L_y \approx 400$ km. In the Bay of Biscay, the large-scale shear flow is on the order of $0.5 \cdot 10^{-7} s^{-1}$ to $10^{-7} s^{-1}$. Here we choose the lower of these two values to assess the effect of shear as a weak perturbation. On figure 6, we show the vortex trajectories: on figure 6a, we kept the same parameters as in the reference case; then, the zonal wavelength of the vortex loops is larger with the shear flow than in its absence (390 km instead of 295) because of the westward advection of the sheared flow. This advection is maximum on the southern part of the trajectories and renders them U-shaped. On figure 6b, we show the simulation which has the same zonal wavelength as the reference simulation, but with shear (the vortices being at the same distance from the coast, $y_c/R_d = 4.67$). To obtain this result, an initial distance between the vortices $d/R_d = 3.33$ is necessary. But the meridional wavelength is only 90 km in this case, therefore less close to observations than the reference case. We conclude that the presence of the shear flow, which renders the loops of the surface vortex more U-shaped, does not provide zonal and meridional wavelength closer to the observations than the reference case (again for equal strength vortices, at the observed distance from the coast).

For a strain flow, we first assume that the Bay of Biscay can be idealized as the second quadrant of the plane ($x < 0, y > 0$) for a center-symmetric strain ($u = s(x - L_x/2), v = -sy$, where L_x is the zonal length of the domain). That is, the eastern boundary of the Bay corresponds to the y-axis of the strain. In this case the flow is directed southwestward in the whole domain. Figure 7 shows the vortex trajectory for a strain rate $0.5 \cdot 10^{-7} s^{-1}$. Clearly, the strain advects the vortices towards the coast but also increases the zonal wavelength of the loops.

Secondly, following Colas (2003; his figure 2.1), we assume that the currents in the south-eastern Bay of Biscay could be directed eastward. To do so, we assume that the Bay of Biscay is the upper half-plane ($y > 0$) for a center-symmetric strain ($u = sx, v = -sy$). In this case the flow is directed southwestward in the western half of the domain, and southeastward in its eastern half.

If the vortices are initially located in the western half of the domain, the conclusions are identical as above. On the contrary, if they are initially in the eastern half of the domain, their evolution depends on the ratio of the strain rate to their vorticity³. The various trajectories when the strain rate is increased are shown on figure 8. The effect of the strain is to disturb the co-rotation of the two vortices and finally to separate them. This effect is moderate on figure 8a where $s = 0.5 \cdot 10^{-7} \text{ s}^{-1}$. It becomes noticeable as soon as the strain rate is doubled (see figure 8b). In fact, both vortices finally drift westward at longer times. This results from the advection of the two vortices towards to the coast, by the strain. When any vortex is close enough to the coast, the westward advection due to the mirror vortex becomes stronger than the eastward advection due to the strain (in the first quadrant). Therefore, all vortices end up in the second quadrant, very close to the coast, and at very large zonal distances. We conclude that a shear flow provides results closer to observations than a strain flow.

3.5 Summary of the point vortex analysis

We derived the motion for the point vortices and a set of simplified equations which apply when the vortices are distant from each other and from the coast.

- We used this simplified set of equations to calibrate the model parameters from in-situ observations. We compared the results of the numerical model with the complete set of equations to observations, firstly with these parameters. In a model with equal layer thicknesses, and for equal strength vortices, the observed trajectories are fairly well reproduced, but with slightly smaller wavelengths and less U-shaped loops than in the Bay of Biscay.
- Increasing the average distance of the two vortices from the coast leads to smaller zonal and longer meridional wavelengths. Increasing the initial distance between the vortices increases both wavelengths.
- If unequal strength vortices are modeled, at the same distance from the coast as in the observations, vertical asymmetry in the trajectories is naturally observed. The surface trajectories are less U-shaped than in the reference case, if the deep vortex is stronger than the surface one.
- Adding a shear flow with parameters fitted on the mean flow in the Bay of Biscay renders the trajectories more U-shaped. But we could not fit both the zonal and meridional wavelengths of the observations with equal strength vortices, at the real distance from the coast, by varying the initial distance between the two vortices. Note that we have not performed simulations where both the ratio of vortex strength and their initial distance would be varied, in the presence of shear, because of the multiplicity of effects.
- Finally, adding a strain flow (corresponding to a quarter plane), again with parameters fitted on those of the Bay of Biscay, has effects comparable to those of adding a shear flow (rendering trajectories more U-shaped, increasing the zonal wavelength), but also bends the trajectories towards the coast. This was not seen in the observations for swoddy F90a, although this type of behaviour might be somehow representative of swoddy F90b that drifted very slowly southwestward in the southeast corner of the Bay of Biscay (see figure 1). Therefore the influence of a large-scale strain field in the Bay of Biscay on the trajectory of F90a is negligible, or is cancelled by other processes. If the strain flow has an axis of meridional symmetry perpendicular to the Spanish coast, all vortex trajectories end up in the western

³it also depends where the vortices lie initially in the eastern half of the domain; but since their westward advection depends on their strength, the problem can be reduced again to the ratio of strain to vorticity

part of the domain, very close to the coast, due to a dominant mirror effect in the long run.

At least three aspects of two-vortex mutual interaction, and of their interaction with a zonal coast, cannot be addressed with point vortices; they will be studied in the following section with finite-area vortices:

- the strong interaction of any vortex with its mirror image under the form of a coherent dipole;
- the possible vertical re-alignment of vortices initially separated horizontally;
- the possible splitting of one vortex in the shear exerted by its companion vortex.

The influence of beta-effect on the evolution of two finite-size vortices is a whole research topic to be explored in another study.

4 Evolution of finite-area vortices in the numerical model

4.1 The numerical model setting and the simulations

We use a numerical model of the two-layer quasi-geostrophic equations to evaluate the influence of a finite size of the two vortices on their propagation, and on their evolution. The numerical model is based on a pseudo-spectral representation of the equations on a bi-periodic spatial grid. The grid is composed of 512 nodes in each horizontal direction, with node spacing of 3 km. Simulations performed with half domain size or horizontal resolution did not show noticeable differences. Potential vorticity was assessed from relative vorticity and the Burger number in the 1990 Bay of Biscay data.

The vortices are much smaller than the domain size to avoid a spurious influence of periodicity. Their potential vorticity is uniform within a disk of radius R . This step function is initially slightly smoothed on its edge to avoid the Gibbs numerical instability. Since numerical dissipation (biharmonic viscosity) was kept at the minimum value for numerical stability, the vortex profile evolves little during a simulation (see for instance figure 10, left column).

The presence of the coast is replaced by mirror vortices. Vortex trajectories are obtained as follows: the potential vorticity peak in each layer is determined and located at each time step. A threshold equal to $4/5$ of this peak value is then used to locate the vortex core. The centroid of this core is used as vortex center. Tests showed that the results are not sensitive to the value of the fraction of peak vorticity as long as it is larger than $1/3$ on the f -plane. Firstly, many simulations were performed with small vortices, distant from the coast and from each other, for comparison with the point vortex model : the results obtained in these cases were similar to the evolutions of point vortices. Figure 9 compares the trajectory of the surface vortex center, in the point vortex model and in the finite-area vortex model, for the reference case. The zonal separation between the two trajectories over one loop is about 30 km, or 10 % of the zonal wavelength. Figure 10a shows the time-series of horizontal maps of potential vorticity in the upper layer for this reference simulation with finite area vortices. Clearly, the vortex becomes elliptical. This deformation contains a part of the energy of the system so that the finite area vortex propagates less rapidly than its counterpart (see also Nycander and Sutyrin, 1992; Sutyrin et al., 1994).

Vortex splitting under the influence of the companion vortex or of the mirror images is evaluated. We consider that partial splitting occurs when the vortex sheds a filament which does not roll into a circular vortex, and that complete splitting occurs when two separate vortices finally exist in the upper layer. No splitting is observed when the vortices come close to the coast or are more than 30 km apart, provided that they are of equal strength. In two-dimensional flows, vortices split apart when the external strain is more intense than about 15% of the peak vorticity (Legras and Dritschel, 1993). A similar result seems to hold here.

Nevertheless, splitting of the surface vortex can occur if the deep vortex is much stronger and exerts a large shear (or strain) on the former. In a series of simulations varying Q_2/Q_1 and R_2/R_1 , surface vortex splitting occurs when $Q_2/Q_1 = 4$ for $R_2/R_1 = 1$ or when $Q_2/Q_1 = 1$ for $R_2/R_1 = 2$. Thus it appears that the ratio of area-integrated potential vorticities $(Q_2 R_2^2)/(Q_1 R_1^2) = 4$ is the limit for vortex splitting. Several simulations were performed to establish a physical criterion for vortex splitting, e.g. by comparing the shear due to the deep vortex to the surface potential vorticity, or the internally and externally induced velocities at the surface vortex rim. But no simple criterion could be established when d/R_1 or h_2/h_1 are varied. Therefore, we cannot as yet provide a general law for vortex splitting in our problem. Figure 10b shows the time series of upper layer potential vorticity in a case of a partial vortex splitting.

Secondly, vertical vortex alignment does not occur, even when the vortices are very close initially. Numerical experiments, decreasing the distance between the two vortices from 30 km to 3 km, do not show their alignment. If the vortex centers are separated by 3 km, this distance remains constant for about 2 months but increases thereafter. The shear created by the other vortices, in particular the mirror images, leads to a progressive separation of the surface and deep vortices. Indeed, previous work has shown that even a weak shear is able to strongly reduce the critical distance for vortex alignment (Perrot and Carton, 2010). Note that a meddy and a swoddy separated by 20 km have been observed (see section 5) and their trajectory did not evidence alignment.

Finally, no strong dipole was formed with the mirror vortices in any of the simulations with $h_1/h_2 = 1$, $R/R_d = 1$, $d/R_d = 4$, when decreasing y_c/R_d from 6 to 2. The vortex trajectories were similar to those of point vortices.

4.2 Summary and comparison to observations

In summary, numerical simulations of finite-area vortices on the f-plane do not evidence vertical alignment for similar strength vortices, even if they are initially very close. The model results do not show vortex pairing with the mirror vortices either, which would lead to zonal propagation along the coast, for vortices with physical characteristics similar to swoddy F90a (with a deep vortex having equal strength and thickness). Surface vortex splitting is observed only when the deep vortex is much stronger. The trajectories shown by the numerical model are cycloidal, as for the point vortices. The comparison of the finite-area surface vortex trajectory with the F90a trajectory is also satisfactory.

The question now arises about the realism of such an interaction. The observations presented in the following section will show that a swoddy and a deep eddy can indeed come in close vicinity in the southeastern Bay of Biscay.

5 Observations and Interactions of two eddies in the Bay of Biscay

CONGAS was a French project, based on a series of cruises in the Bay of Biscay, between 2004 and 2007, and aiming at measuring the dynamics on and near the continental slope. These cruises comprised CTD stations, with sensors calibrated before and after the cruise. XBT and XCTD probes were cast, but since they were not calibrated, their data must be considered mostly to reveal anomalies than as absolute values. These measurements revealed several mesoscale eddies. In this paper, we focus on two eddies observed at different depths, whose horizontal distance was sufficiently small (less than one internal radius of deformation apart) to assume a mutual dynamical interaction (see above). This mutual interaction is shown by the curvature of the surface vortex (swoddy) trajectory, which will be shown below.

The deepest eddy core was found at around 1000 meter depth, which corresponds to the Mediterranean Water level in that region. This eddy, called a MEDDY (for MEDiterranean edDY, see for example Armi and Zenk, 1984), was observed twice, at a two-week interval. Figure 11 shows a zonal-vertical transect of salinity (from CTD stations and XCTD casts) through the core of this meddy. The overall horizontal extent of this meddy was about 60 km, with a maximum value of salinity of about 36.08 at 1120 m depth. Calculation of the geostrophic currents across the transect (not shown here) indicates that the eddy was anti-cyclonic, with typical maximum azimuthal velocities around 25 cm/s around 1000 m depth. In addition, the use of SIPPICAN XCTD probes allowed to cover a wide area around and inside the eddies during the two periods of measurements. Figures 12a and 12b show the horizontal salinity at 1000 m depth, for the two periods, as obtained from CTD and XCTD casts. During the first leg, a lens of higher salinity is isolated from its surrounding and corresponds to the meddy, with salinity anomaly of 0.2-0.3 compared to its environment (Figure 12a). This lens appears asymmetric, with a slightly meridional orientation. Ten days later (Figure 12b), the core of the meddy had evolved, showing a reduction of its salinity and of its diameter. A small part of the core also seems to have been snatched toward the northern part of the meddy, but unfortunately, we have no measurement in this region during the previous leg.

Another eddy, shallower than the first one was observed during the second leg of the cruise (Figure 12c). This eddy has a temperature maximum of 11.90°C at 168 m depth and a salinity maximum of 35.67 at 175 m depth (as measured with a CTD). This anticyclonic structure, which we could assimilate to a SWODDY (after Pingree and Le Cann, 1992), was horizontally located northeast of the meddy, at a distance of about 20 km (estimated core to core). Three drifting buoys, two tethered (2.1 mm diameter cable) with a holeysock drogue 1 m wide and 12 m long at 75 m depth, and one tethered (1.7 mm diameter cable) with a similar holeysock at 200m depth, were deployed near the center of this eddy. Two months (61 days) of the raw trajectory of the 200 m drogued buoy are displayed on figure 13. The trajectories of the buoys drogued at 75 m are similar and not shown for clarity. The buoy trajectory clearly exhibits, in addition to high-frequency (mostly semi-diurnal) motions, anticyclonic loops associated with the trapping in the swoddy, with typical 3-4 day periods, and maximum azimuthal velocities around 25 cm/s. From this raw trajectory, we estimated the trajectory of the center (in red on Figure 13) of these loops, with the method described

in Paillet et al, 2002. We note that this swoddy center track itself exhibits a cycloidal motion with anticyclonic loops, with typical 20 day period and about 15 km amplitude, superposed on a general motion, first southward and then westward. This looping center behaviour, already noticed in Paillet et al, 2002, and Reverdin et al, 2009, and the general southward then westward center motion, might be interpreted as resulting from the interaction with the underlying meddy. We have no indication though of the trajectory of the meddy center during the same period.

Note that the cycloidal trajectory observed here is different from that simulated on the f -plane, with two equal strength vortices in the quasi-geostrophic model. In this case, the modelled trajectory is cycloidal with a mean zonal drift. Numerical simulations on the beta-plane lead to a similar trajectory for the surface vortex, if the two vortices have a maximum velocity on the order of 16 cm/s (if they have equal strength). Vertical alignment of the meddy and swoddy did not occur in any of the two cases (observation and model). These observations support the likelihood of meddy-swoddy interactions in the southern Bay of Biscay.

6 Further evidence of Meddies in the Bay of Biscay

In order to further investigate positive salinity anomalies at MW level in the Bay of Biscay, we examined the ARGO profiles available in the area. These profiles were downloaded from the Coriolis site (<http://www.coriolis.eu.org>) in May 2010. We selected the profiles with both temperature and salinity data. These profiles were compared with the high resolution GHER climatological atlas for the NorthEast Atlantic (Troupin et al, 2010). Other climatologies (e.g. World Ocean Database 2005) gave similar results (although anomaly values would vary, as the different climatologies differ in data content and processing). We scanned the profiles for positive salinity anomalies, greater than 0.2 in the 700-1300 m depth range (a criterion similar to, but slightly weaker than the one used by Richardson et al (1991)). Temperature and salinity profiles were individually checked, through comparison with climatology, and also for static stability. Although no in situ calibration is available, we estimate that salinity error is less than 0.05, from comparison with climatological data outside the MW range.

Figure 14 shows the results of this exploration: a dense cluster of anomalies in the South-west corner, around $44 - 45^{\circ}\text{N}$, $8 - 9^{\circ}\text{W}$. Most of these anomalies are likely to correspond to observations of "Northern Meddies" (Paillet et al, 2002). East of 7°W , a few salinity anomalies, detached from the slopes, are found near $45 - 46^{\circ}\text{N}$, $6 - 7^{\circ}\text{W}$. Two of these salinity anomalies are interpreted as indicating the presence of a Meddy.

Anomaly # 1 was sampled by float # 4900557 in March-April 2006 (Figures 14 and 15), and was intensified between 1000-1300 m depths (maximum salinity anomaly equal to 0.23 at 1250 m). At its maximum (cycle # 56), the salinity anomaly extended from about 700 m to 1400 m deep. Temperature anomalies were associated with salinity anomalies, roughly in the ratio 1°C for 0.2.

Anomaly # 2 was sampled by float # 6900363, from December 2008 to April 2009 (Figures 14 and 16), and had characteristics similar to anomaly # 1 (maximum salinity anomaly 0.24

at 1280 m). During that period, float 6900363, ballasted for about 1000 m depth, first moved eastward along the continental slope near 8°W , and then abruptly left the slope near 7.5°W . It then slowly moved in a general northeastward direction (Figure 14), at speeds of about 3.5 cm/s. Salinity anomalies are intensified on the slope and then in the northeastern part of the track, most likely as a result of sampling. While following the salinity anomaly at depth, the float may slightly move in or out of the salinity maximum, as it surfaces every 10 days, and is thus displaced. The abruptness with which the float left the slope is a possible indication of an interaction with another eddy.

In summary, selected observations show that noticeable salinity anomalies at MW level exist in the Bay of Biscay, near the locations where swoddies were observed in 1990 and during the CONGAS cruises. Such anomalies, able to trap floats and to move in a coherent manner, can be interpreted as meddies.

7 Summary, discussion and conclusions

From the observation of the cycloidal trajectory of swoddy F90a, we conducted a vortex dynamics study in the simplest framework compatible with the observations: a two-layer quasi-geostrophic model, which allows vortex baroclinicity, or the presence of vortices in different layers.

Firstly, we analyzed the motion of two point vortices on the f -plane in the presence of a zonal coast, these vortices being like-signed and located in different layers. When the vortices are much farther from the coast than from each other, their motion can be reduced to the addition of a mutually induced rotation and of a uniform zonal translation due to the mirror vortices. The zonal velocity obtained in this case is comparable with that observed in the Bay of Biscay for F90a (about 2 cm/s). The meridional extent of the loop is also close to the distance between the vortices. This extent being much larger than a typical vortex radius indicates that the swoddy must have been influenced by a distinct deep vortex (in the case of equal vortex strengths and equal layer depths). A comparison of the vortex trajectories in the model with observations shows qualitative agreement. Bringing the vortices closer to the coast modifies the trajectories, amplifies the zonal drift and reduces the meridional extent of the loops (the "meridional wavelength"). This extent is also amplified in the upper layer if this layer is thinner than the lower one, or if the deep vortex is stronger than the surface one. Again, this corresponds to two distinct vortices and not to a single, tilted, vortex. Finally, this investigation of the motion of two point vortices was complemented by experiments on the influence of a large-scale shear or strain flow. The addition of a shear flow renders the trajectories U-shaped. The addition of a strain flow induces a global drift towards the coast, in addition to modifying the zonal and meridional wavelengths.

Secondly, we investigated the effect of a finite vortex size on its trajectory and evolution, on the f -plane. We found that, under realistic conditions (i.e. to fit the F90a observations), vortex splitting or vertical re-alignment were unlikely. Nevertheless, surface vortex splitting is possible if the deep vortex is intense. No strong pairing of the vortex with its mirror image, as a coherent dipole, occurred. Comparison of model results with the F90a

observations, indicates again that the surface and deep vortices must have been separated by 3 to 4 deformation radii as they interacted (if they were of similar strength and thickness).

To support this interpretation of the looping trajectory of F90a as the result of deep vortex-surface vortex interaction, complementary data were analysed. Firstly, hydrological and float data from CONGAS showed the presence of a meddy and a swoddy in close vicinity near 45°N, 8°W. Their deformation and the motion of the swoddy indicate that they were interacting. We also searched in the ARGO profiler database, for long-lasting, intense salinity anomalies at the MW level, with coherent trajectories. We analysed such anomalies, showing that they could last several months, that they were born on the continental slope and that they could drift northeastward, i.e. towards the region of generation of swoddy F90a (Cape Ferret canyon).

Though the association of all our model results and in-situ observations reasonably support the hypothesis of meddy-swoddy interaction to explain the trajectory of F90a, many unknowns remain about the exact structure and location of this hypothetical meddy. In particular, other effects can replace the influence of the coast, west of 9°W, such as large-scale zonal flows, or the influence of cyclonic vortices.

On the one hand, we acknowledge that our model is very idealized and that more realism could be attained by considering a finer vertical resolution, or also, by using a shallow-water, primitive equation model. The trade-off of such models is that we lack data to fine-tune their initial conditions to which they are quite sensitive. On the other hand, our data are limited in space and time: we do not have information of the deep motions around swoddy F90a which could ascertain the presence of a meddy. We do not either have a complete 3D view of the salinity anomalies related to the ARGO float measurements. Therefore, in the future, dedicated in-situ observations should be carried out when a cycloidal vortex trajectory is observed via remote sensing.

Acknowledgements

We acknowledge support from UBO, from CNRS and from SHOM during the course of this study. We also acknowledge the help of Patrice Bellec from LPO for the processing of ARGO floats profiles and the GHA group and IES department from SHOM.

References

- Armi L., Zenk W., 1984: Large lenses of highly saline Mediterranean Water. *J. Phys. Oceanogr.*, **14**, 1560-1576.
- Bertrand C., Carton X.J., 1993: Vortex merger on the beta-plane. *Compte-Rendus Acad. Sc. Paris*, **t.316**, II, 1201-1206.
- Carton X., Chérubin L., Paillet J., Morel Y., Serpette A., Le Cann B., 2002: Meddy coupling with a deep cyclone in the Gulf of Cadiz. *J. Mar. Syst.*, **32**, (1-3), 13-42.
- Carton X., 2001: Hydrodynamical modeling of oceanic eddies. *Surveys in Geophysics*, **22**, 3, 179-263.
- Colas F., 2003: Circulation et dispersion lagrangienne en Atlantique nord est. *Thèse de*

- doctorat de l'Université de Bretagne Occidentale, Brest, France, **943**, 259 pp.
- Dubert, J.M., 1993: Le SWODDY est il un heton ? *MSc Research Report*, Rapport de stage du DEA Oceans. Université de Bretagne Occidentale, Brest, France.
- Frouin R., Fiuza A.F.G., Ambar I., Boyd T.J., 1990: Observations of a Poleward Surface Current off the coasts of Portugal and Spain during winter. *J. Geophys. Res.*, C, **95**, 679691.
- Garcia-Soto C., Pingree R.D., Valdés L., 2002: Navidad development in the southern Bay of Biscay: Climate change and swoddy structure from remote sensing and in situ measurements. *J. Geophys. Res.*, **107**, 3118, 29 pp., doi:10.1029/2001JC001012.
- Haynes R., Barton E.D., 1990: A poleward flow along the Atlantic coast of the Iberian peninsula. *J. Geophys. Res.*, C, **95**, 11425-11441.
- Hogg N.G., Stommel H.M., 1985: The Heton, an Elementary Interaction Between Discrete Baroclinic Geostrophic Vortices, and Its Implications Concerning Eddy Heat-Flow. *Proc. Royal Soc. London, Series A*, **397**, 1812, 1-20.
- Koutsikopoulos C., Le Cann B., 1996: Physical processes and hydrological structures related to the Bay of Biscay anchovy. *Sci. Mar.*, **60**, Suppl.2, 9-19.
- Le Cann B., Serpette A., 2009: Intense warm and saline upper Ocean inflow in the southern Bay of Biscay in autumn-winter 2006-2007. *Cont. Shelf Res.*, **29**, 1026-1037.
- Legras B., Dritschel D.G., 1993: Vortex stripping and the generation of high vorticity gradients in two-dimensional flows. *Applied Sci. Res.*, **51**, 445-456.
- Morel Y., Thomas L., 2009: Ekman drift and vortical structures. *Ocean Model.*, **27**, 185-197.
- Nycander J., Sutyrin G.G., 1992: Steadily translating anti-cyclones on the beta plane. *Dyn. Atmos. Oceans*, **16**, 473-498.
- Paillet J., Le Cann B., Serpette A., Morel Y., Carton X., 1999: Real-time tracking of a northern meddy in 1997-98. *Geophys. Res. Lett.*, **26**, 13, 1877-1880.
- Paillet J., Le Cann B., Carton X., Morel Y., Serpette A., 2002: Dynamics and evolution of a northern Meddy. *J. Phys. Oceanogr.*, **32**, 55-79.
- Perrot X., Carton X., 2010: Geostrophic vortex alignment in external shear or strain. *Proceedings of the IUTAM Symposium on Turbulence in the Atmosphere and Oceans*, Springer Verlag, 217-228.
- Pingree R.D., 1993: Flow of surface waters to the west of the British Isles and in the Bay of Biscay. *Deep-Sea Res.*, **40**, 369-388.
- Pingree R.D., Le Cann B., 1989: Celtic and Armorican shelf and slope residual currents. *Progress in Oceanography*, **23**, 303-338.
- Pingree R.D., Le Cann B., 1990: Structure, strength and seasonality of the slope currents in the Bay of Biscay region. *Journal of the Marine Biological Association of the United Kingdom*, **70**, 857-885.
- Pingree R.D., Le Cann B., 1992a: Three anticyclonic Slope Water Oceanic eDDIES (SWODDIES) in the southern Bay of Biscay in 1990. *Deep-Sea Res.*, **39**, 1147-1175.
- Pingree R.D., Le Cann B., 1992b: Anticyclonic Eddy X91 in the Southern Bay of Biscay, May 1991 to February 1992. *J. Geophys. Res.*, **97**, C9, 14353-14367.
- Reverdin G., Gascard J.C., Le Cann B., Prieur L., Assenbaum M., Lherminier P., 2009: A Long-Lasting Mode Water Vortex in the Northeast Atlantic Ocean. *J. Phys. Oceanogr.*, **39**, 536-558.
- Richardson, P.L., M.S. McCartney, Maillard C., 1991: A search for meddies in historical data. *Dyn. Atmos. Oceans*, **15**, 241-265.
- Serpette A., Le Cann B., Colas F., 2006: Lagrangian circulation of the North Atlantic Cen-

tral Water over the abyssal plain and continental slopes of the Bay of Biscay: description of selected mesoscale features. *Scientia Marina*, **70**, doi:10.3989/scimar.2006.70s127.

Sutyrin G.G., Hesthaven J.S., Lynov J.P., Rasmussen J.J., 1994: Dynamical properties of vortical structures on the beta-plane. *J. Fluid Mech.*, **268**, 103-131.

Troupin C., Machín F., Ouberdous M., Sirjacobs D., Barth A., Beckers J.M., 2010: High-resolution Climatology of the North-East Atlantic using Data-Interpolating Variational Analysis (Diva). *J. Geophys. Res.*, *115*, doi:10.1028/2009JC005512.

Zabusky N.J., McWilliams J.C., 1982: A modulated point vortex for geostrophic, beta-plane dynamics. *Phys. Fluids*, **25**, 12, 2175-2182.

List of figure captions

Fig.1: Trajectory of Swoddy F90a center from 1989/12/29 until 1990/10/06, plotted as red dots and track. Crosses, labelled by letters, are the estimated positions of the eddy center on the first day of the month indicated. The tracks of Swoddies F90b and O90a are resp. plotted as empty squares and triangles. Figure adapted from Pingree and Le Cann, 1992a, their figure 5.

Fig.2: Schematic diagram of the two-eddy configuration north of the coast, with the relevant dynamical parameters for the point-vortex and finite-area vortex studies. R is the vortex radius, Q_a and Q_b are the vortex charges (or strengths, see text), H_1 and H_2 are the layer thicknesses, and x_a, y_a, x_b, y_b are the coordinates of the two vortex centers.

Fig.3: (a) (top) Point vortex trajectories in the two layers (v1=surface vortex, v2=deep vortex) for $(h_1Q_a)/(h_2Q_b) = 1, d/R_d = 4, y_c/R_d = 4.67$; axes are graduated in km, using $R_d = 30$ km; (b) (middle) Comparison of the theoretical estimate of the "zonal wavelength" λ_x (that is, the zonal displacement of the surface vortex), with that measured in the numerical point vortex model, with respect to y_c ; (c) (bottom) meridional displacement λ_y of the vortices in the numerical model, with respect to y_c . Note that for large y_c , the asymptotic value for both λ_x and λ_y , is d (here 120 km).

Fig.4: (a) (top) "Zonal wavelength" in the numerical point-vortex model, with respect to d for $(h_1Q_a)/(h_2Q_b) = 1, y_c/R_d = 4.67$; axes are graduated in km, using $R_d = 30$ km; (b) (bottom) meridional displacement λ_y of the vortices in the numerical point-vortex model, with respect to d .

Fig.5: (a) Point vortex trajectories in the two layer for $(h_1Q_a)/(h_2Q_b) = 1, d/R_d = 4, y_c/R_d = 4.67$; axes are graduated in km, using $R_d = 30$ km (top); (b) same as (a) for $(h_1Q_a)/(h_2Q_b) = 0.5, d/R_d = 4, y_c/R_d = 4.67$ (middle); (c) same as (a) for $(h_1Q_a)/(h_2Q_b) = 0.67, d/R_d = 4.5, y_c/R_d = 4.67$ (bottom).

Fig.6: Point vortex trajectories in the two layers for $(h_1Q_a)/(h_2Q_b) = 1, y_c/R_d = 4.67$ with shear amplitude $s = 0.5 \cdot 10^{-7} s^{-1}$; axes are graduated in km, using $R_d = 30$ km; (a) case with $d/R_d = 4$ (top); (b) case with $d/R_d = 3.33$ (bottom).

Fig.7: Point vortex trajectories in the two layers for $(h_1Q_a)/(h_2Q_b) = 1, d/R_d = 4, y_c/R_d = 4.67$ and with a strain rate $s = 0.5 \cdot 10^{-7} s^{-1}$; the strain flow is centered in the Southeastern corner of the Bay of Biscay (i.e. the associated flow is westward along the whole Northern Spanish coast); axes are graduated in km, using $R_d = 30$ km. Two streamlines of the strain are plotted in dotted lines.

Fig.8: Point vortex trajectories in the two layers for $(h_1Q_a)/(h_2Q_b) = 1, d/R_d = 4, y_c/R_d = 6$ and with a strain rate $s = 0.5 \cdot 10^{-7} s^{-1}$ (top) and $s = 10^{-7} s^{-1}$ (bottom). The strain flow is now centered in the middle of the Spanish coast, so that currents are eastward/westward in the southeastward/southwestward Bay of Biscay; axes are graduated in km, using $R_d = 30$ km. Two streamlines of the strain are plotted in dotted lines.

Fig.9: Comparison of the point vortex and finite area vortex trajectories in the upper layer, for the reference case (see also figure 3a); axes are graduated in km, using $R_d = 30$ km.

Fig.10: Time series of potential vorticity maps in the upper layer for the reference experiment (left column) and for another experiment with the same parameters except $Q_2/Q_1 = 4$ (right column). The reference experiment shows that the vortex shape remains little changed during its evolution, whereas in the other experiment, substantial filamentation (or partial splitting) occurs. Times (from top to bottom) are $t = 0, 20, 40, 60, 80$ days.

Fig.11: Zonal vertical salinity transect through the Meddy and the Swoddy cores. CTD measurements are from 2005/07/18 to 2005/07/19 (leg 2) at around $45^{\circ}03'N$. The westernmost point of measurement corresponds to a XCTD profile, obtained at the end of 2005/07/17.

Fig.12: (a) Horizontal map of salinity at 1000 m obtained from CTD and XCTD measurements between 2005/07/01 and 2005/07/04 (leg 1). Grey contour is for the 1000 m isobath. (b) Horizontal map of salinity at 1000 m obtained from CTD and XCTD measurements between 2005/07/16 and 2005/07/19 (leg 2). Grey contour is the same as in (a). (c) Horizontal map of temperature at 200 m obtained from CTD and XCTD measurements between 2005/07/16 and 2005/07/19 (leg 2). Grey contour is for the 200 m isobath. Temperature map was preferred to salinity map, due to noise in XCTD data. Red dots indicate the position of CTD stations, while small black dots are for the XCTD measurements.

Fig.13: Black track: raw trajectory of buoy #30666 drogued at 200 m, deployed on 19/07/2005 (black cross at the center of large magenta spot). Black crosses along the black track are daily marks. The magenta (cyan) large dot circled in black indicate the position of the swoddy (meddy) core estimated from CTD/XCTD measurements at the beginning of the buoy track. The red track is the trajectory of the swoddy center, estimated from the buoy track (with red dots every 5 days).

Fig.14: Map of salinity anomalies in the 700-1300 m range in the Bay of Biscay, derived from the analysis of ARGO floats up to May 2009 (see text). Positive salinity anomalies greater than 0.2 are plotted, as cyan, red and black dots. The area of the dots is proportional to strength of the anomaly. Salinity anomalies less than 0.2 are plotted, as blue points. Float # 4900557 anomaly # 1 (cycle 56, 2006/03/28) is plotted as a black dot. Float # 6900363 anomalies (anomaly # 2) are plotted as a red dots (from cycle 126, 2008/12/13, to cycle 137, 2009/04/02). Float # 6900363 underwater trajectory (between diving and surfacing points) is plotted as red solid 10 day segments. First diving point (2008/12/13) is indicated as a large downward pointing blue triangle and last surfacing position (2009/04/02) is indicated as a large upward pointing blue triangle.

Fig.15: Individual vertical profiles for float # 4900557 (anomaly # 1, black dot in Figure 14). a) Temperature profiles as a function of depth. b) Salinity profiles as a function of depth. On each of the plots a and b: on the right of each figure, solid lines denote profiler data and dashed lines the monthly climatological profiles at the closest location (Troupin et al, 2010) with the scale at bottom of plot; on the left of each plot, are plotted the anomalies (profiler data minus monthly climatological data), with the scale at top of plot. Lines are color-coded as a function of cycle number (from cycle 53 (2006/02/26) to cycle 58 (2006/04/17)).

Fig.16: Same as for Figure 15 but for float # 6900363 (anomaly # 2, red dots and segments in Figure 14). Lines are color-coded as a function of cycle number (from cycle 126 (2008/12/13) to cycle 137 (2009/04/02)).

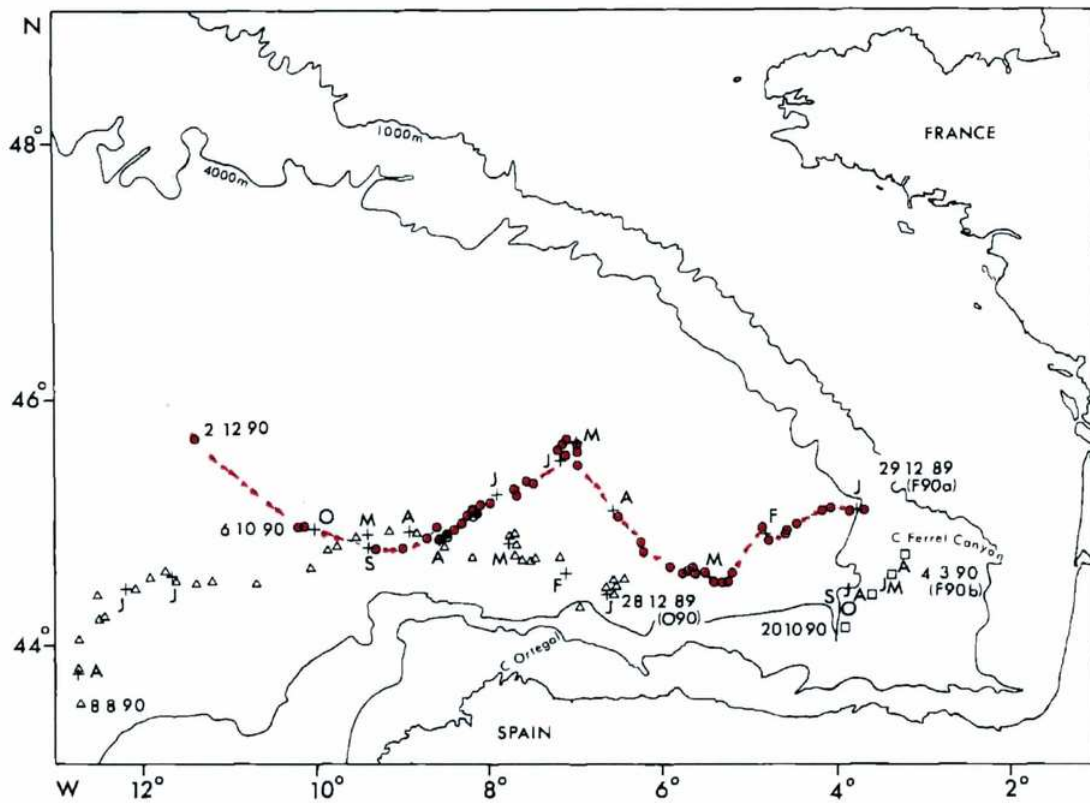


Figure 1: Trajectory of Swoddy F90a center from 1989/12/29 until 1990/10/06, plotted as red dots and track. Crosses, labelled by letters, are the estimated positions of the eddy center on the first day of the month indicated. The tracks of Swoddies F90b and O90a are resp. plotted as empty squares and triangles. Figure adapted from Pingree and Le Cann, 1992a, their figure 5.

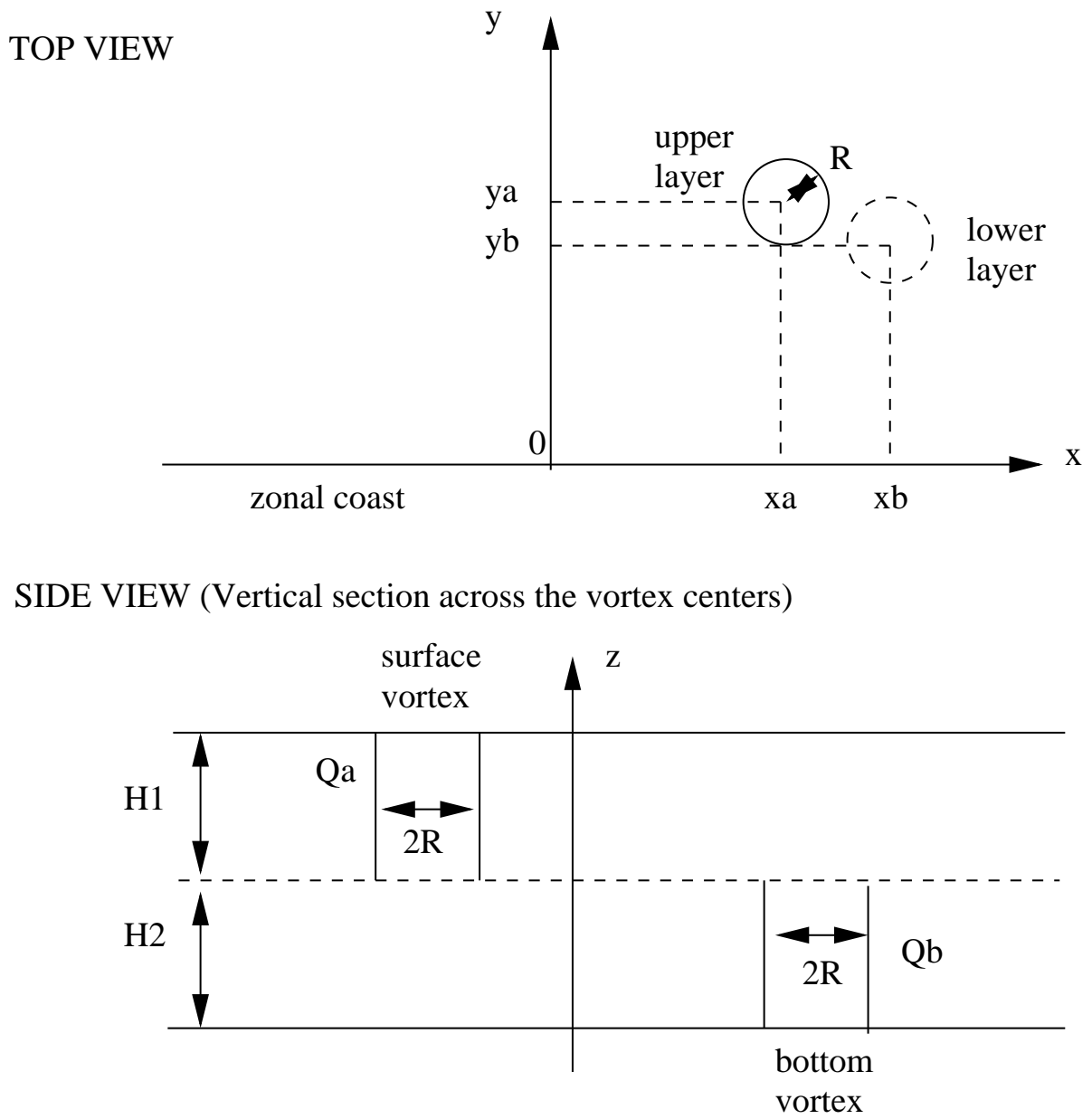


Figure 2: Schematic diagram of the two-eddy configuration north of the coast, with the relevant dynamical parameters for the point-vortex and finite-area vortex studies. R is the vortex radius, Q_a and Q_b are the vortex charges (or strengths, see text), H_1 and H_2 are the layer thicknesses, and x_a, y_a, x_b, y_b are the coordinates of the two vortex centers.

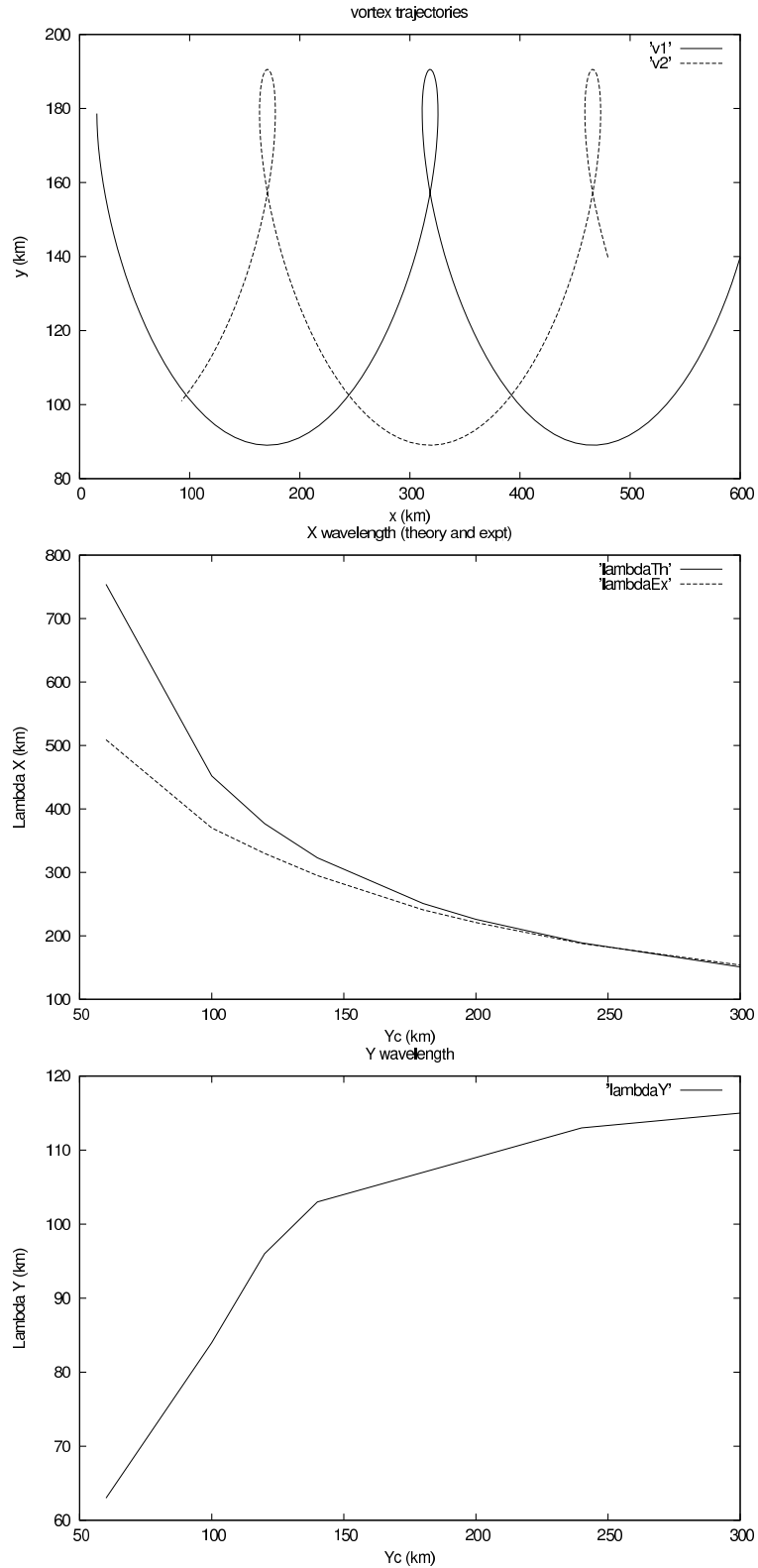


Figure 3: (a) (top) Point vortex trajectories in the two layers (v_1 =surface vortex, v_2 =deep vortex) for $(h_1 Q_a)/(h_2 Q_b) = 1$, $d/R_d = 4$, $y_c/R_d = 4.67$; axes are graduated in km, using $R_d = 30$ km; (b) (middle) Comparison of the theoretical estimate of the "zonal wavelength" λ_x (that is, the zonal displacement of the surface vortex), with that measured in the numerical model, with respect to y_c ; (c) (bottom) meridional displacement λ_y of the vortices in the numerical point-vortex model, with respect to y_c . Note that for large y_c , the asymptotic value for both λ_x and λ_y , is d (here 120 km)²⁴

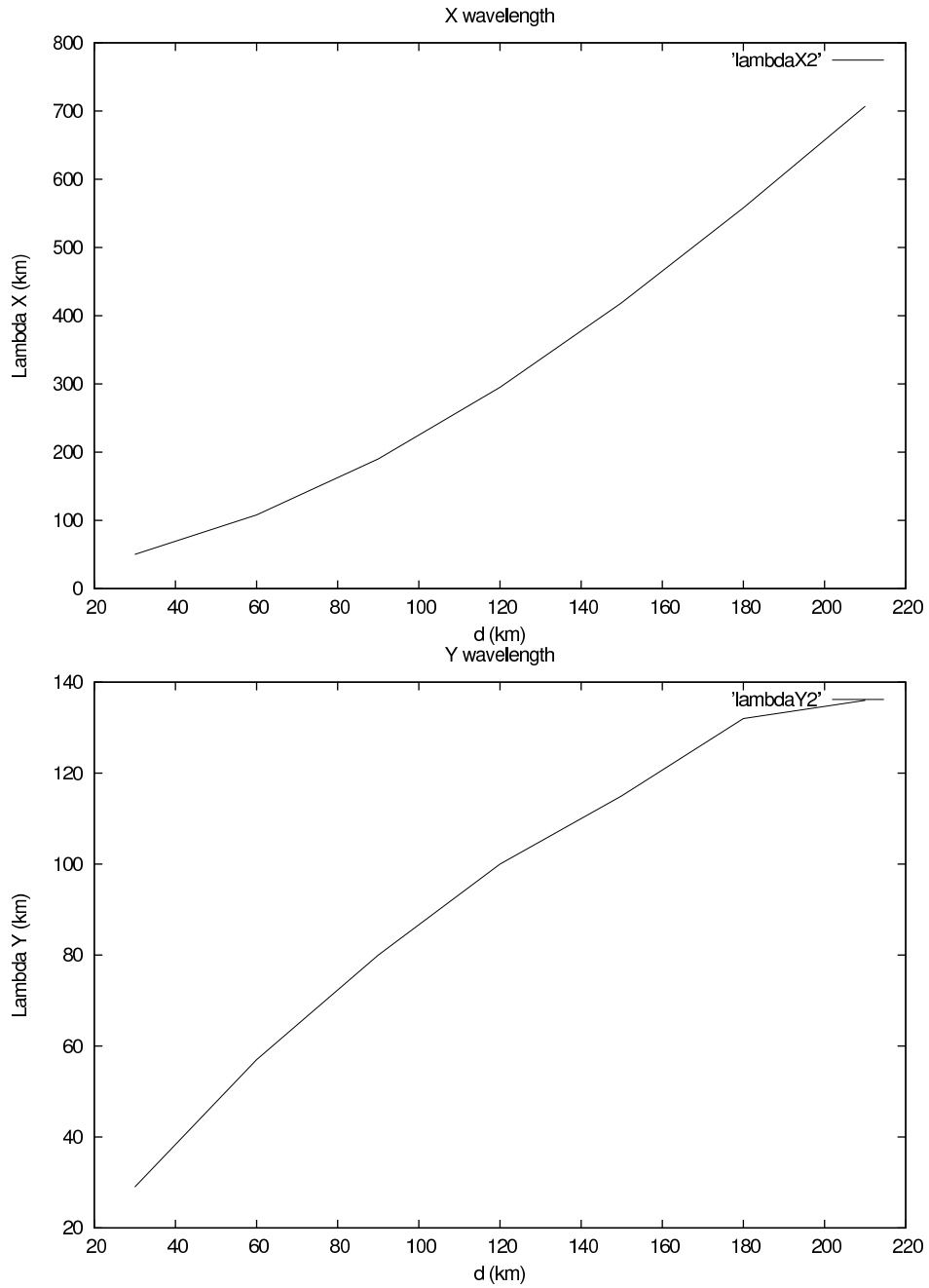


Figure 4: (a) (top) "Zonal wavelength" in the numerical point-vortex model, with respect to d for $(h_1 Q_a)/(h_2 Q_b) = 1$, $y_c/R_d = 4.67$; axes are graduated in km, using $R_d = 30$ km; (b) (bottom) meridional displacement λ_y of the vortices in the numerical point-vortex model, with respect to d .

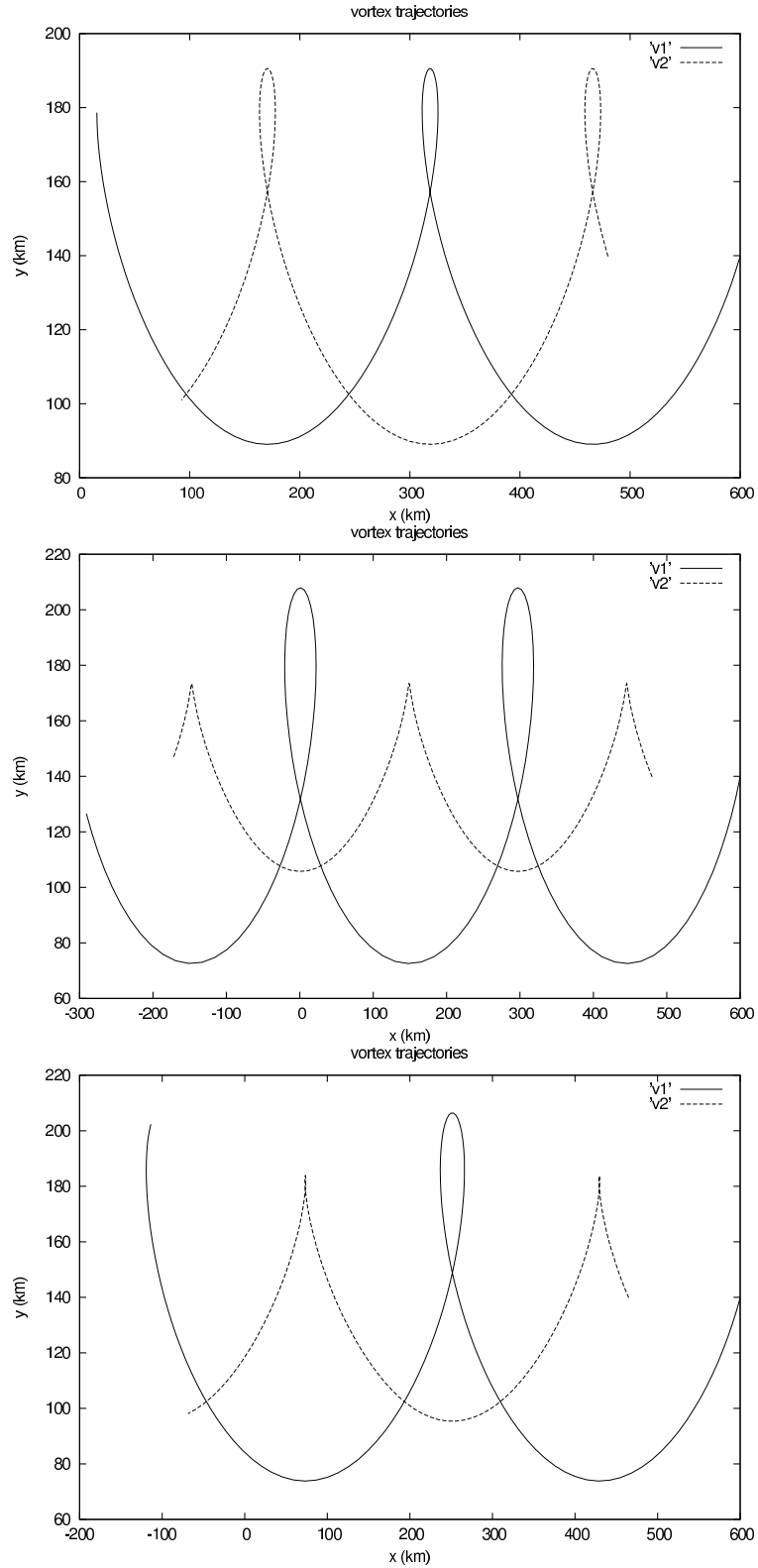


Figure 5: (a) Point vortex trajectories in the two layer for $(h_1 Q_a)/(h_2 Q_b) = 1, d/R_d = 4, y_c/R_d = 4.67$; axes are graduated in km, using $R_d = 30$ km (top); (b) same as (a) for $(h_1 Q_a)/(h_2 Q_b) = 0.5, d/R_d = 4, y_c/R_d = 4.67$ (middle); (c) same as (a) for $(h_1 Q_a)/(h_2 Q_b) = 0.67, d/R_d = 4.5, y_c/R_d = 4.67$ (bottom).

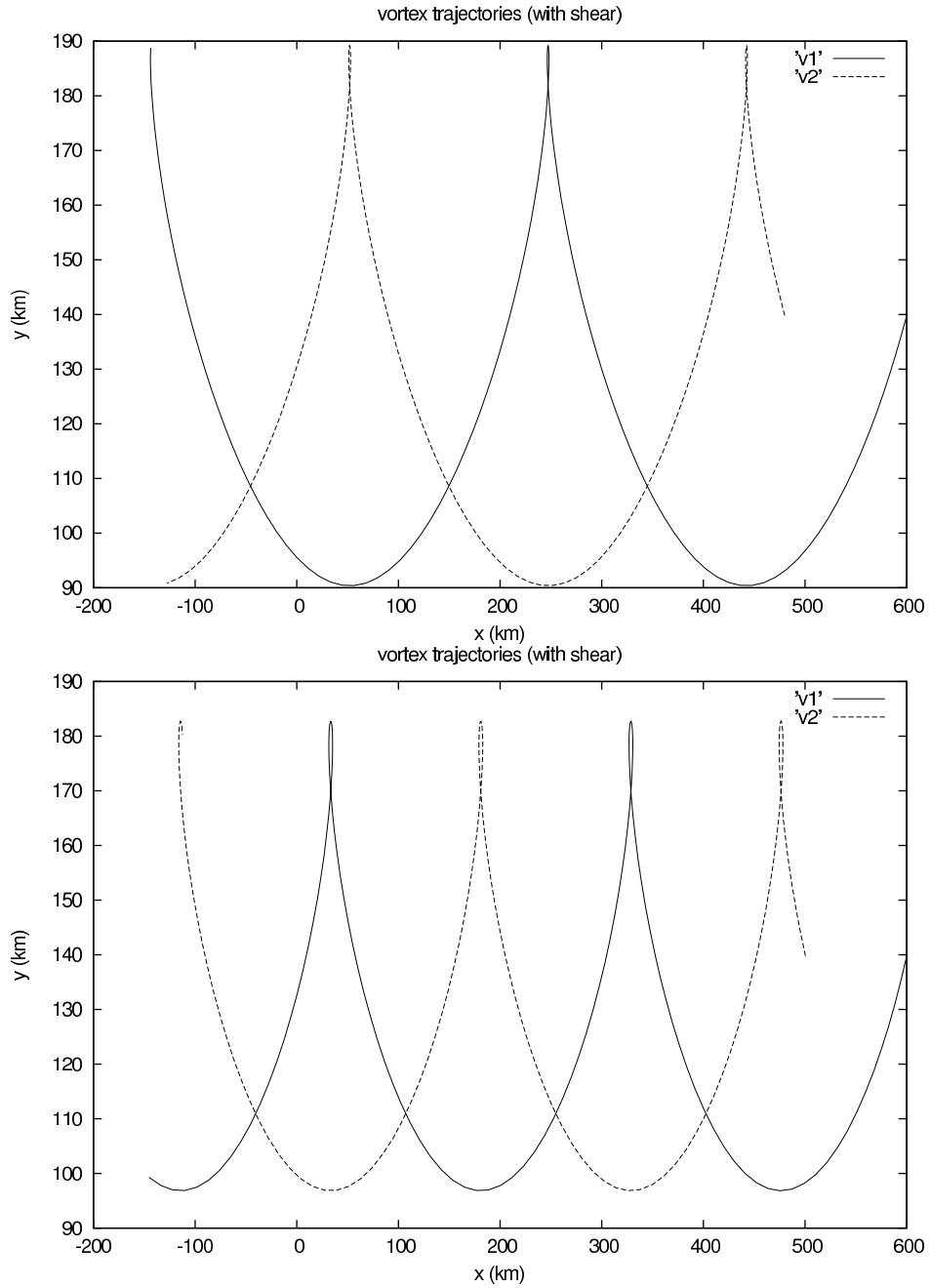


Figure 6: Point vortex trajectories in the two layers for $(h_1 Q_a)/(h_2 Q_b) = 1$, $y_c/R_d = 4.67$ with shear amplitude $s = 0.5 \cdot 10^{-7} s^{-1}$; axes are graduated in km, using $R_d = 30$ km; (a) case with $d/R_d = 4$ (top); (b) case with $d/R_d = 3.33$ (bottom).

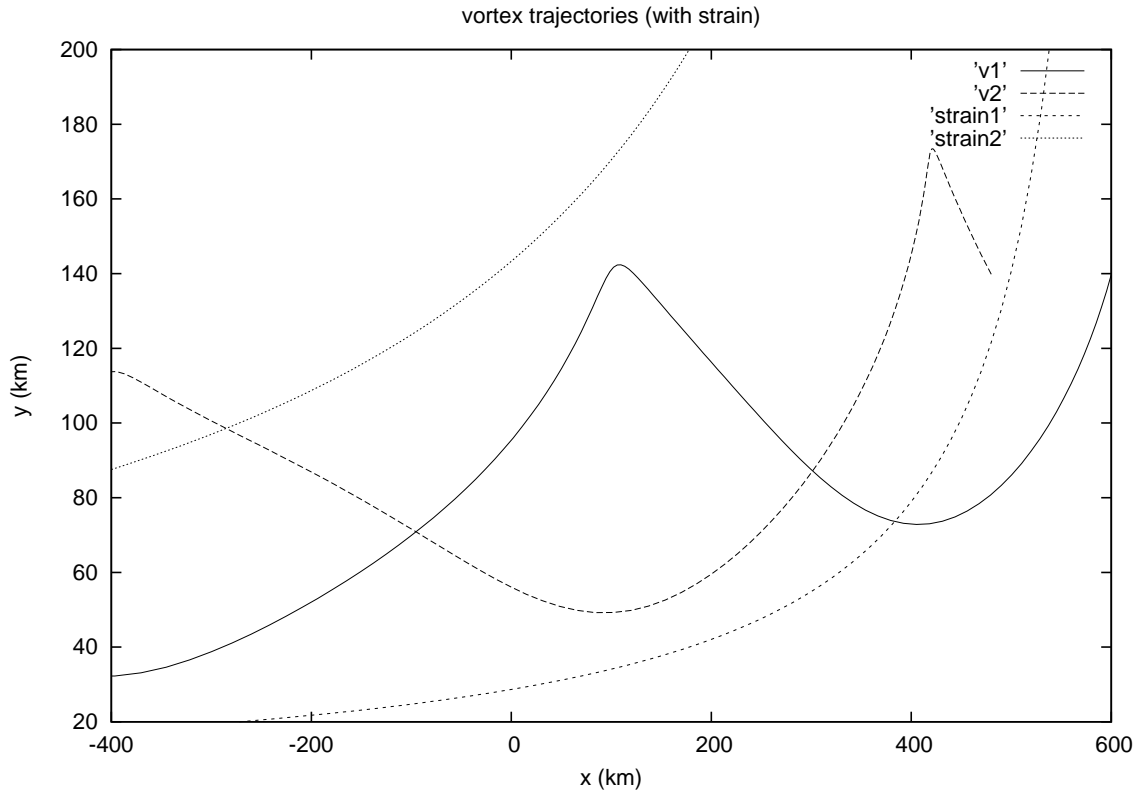


Figure 7: Point vortex trajectories in the two layers for $(h_1 Q_a)/(h_2 Q_b) = 1$, $d/R_d = 4$, $y_c/R_d = 4.67$ and with a strain rate $s = 0.5 \cdot 10^{-7} s^{-1}$; the strain flow is centered in the Southeastern corner of the Bay of Biscay (i.e. the associated flow is westward along the whole Northern Spanish coast); axes are graduated in km, using $R_d = 30$ km. Two streamlines of the strain are plotted in dotted lines.

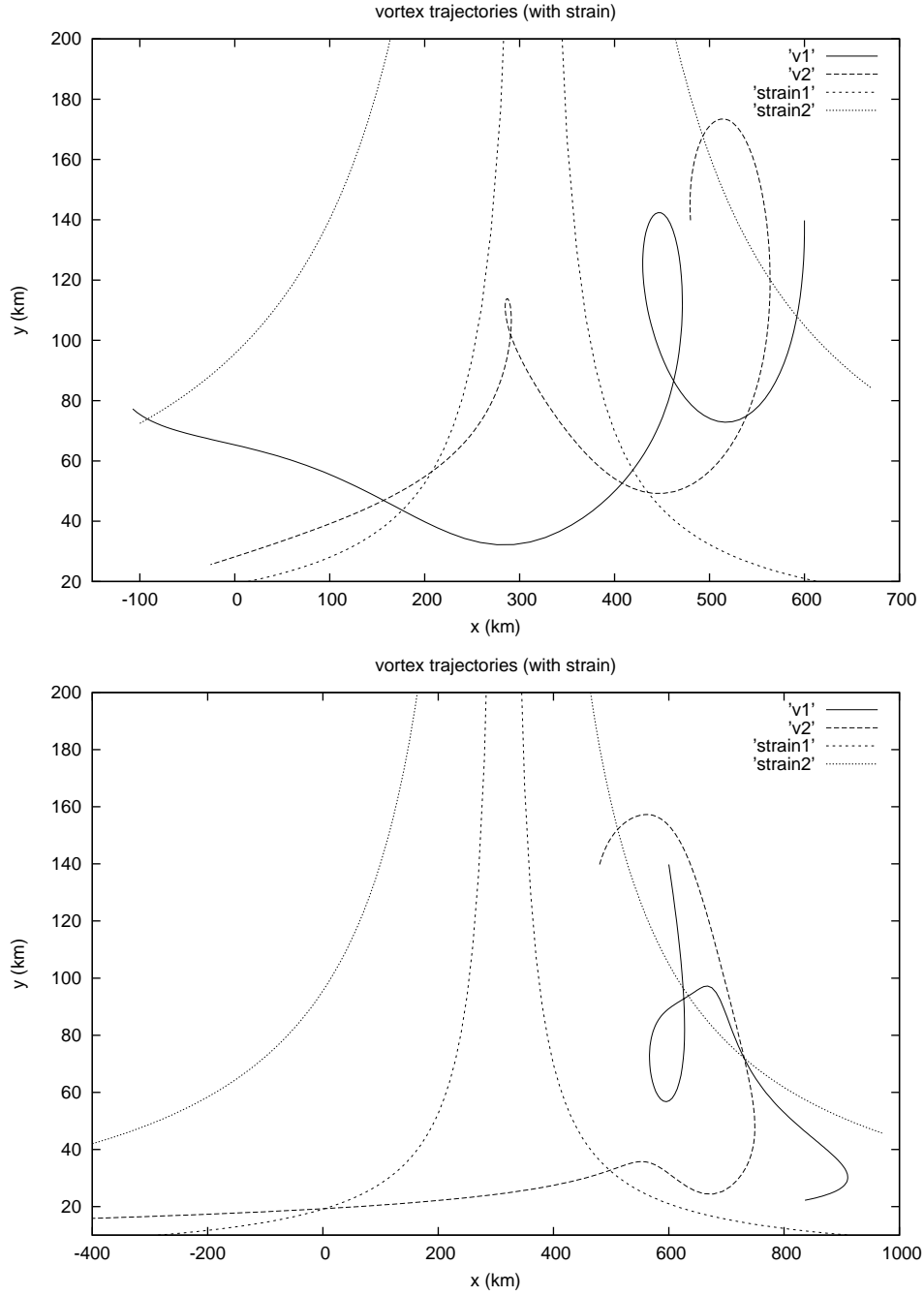


Figure 8: Point vortex trajectories in the two layers for $(h_1 Q_a)/(h_2 Q_b) = 1$, $d/R_d = 4$, $y_c/R_d = 6$ and with a strain rate $s = 0.5 \cdot 10^{-7} \text{ s}^{-1}$ (top) and $s = 10^{-7} \text{ s}^{-1}$ (bottom). The strain flow is now centered in the middle of the Spanish coast, so that currents are eastward/westward in the southeastward/southwestward Bay of Biscay; axes are graduated in km, using $R_d = 30 \text{ km}$. Two streamlines of the strain are plotted in dotted lines.

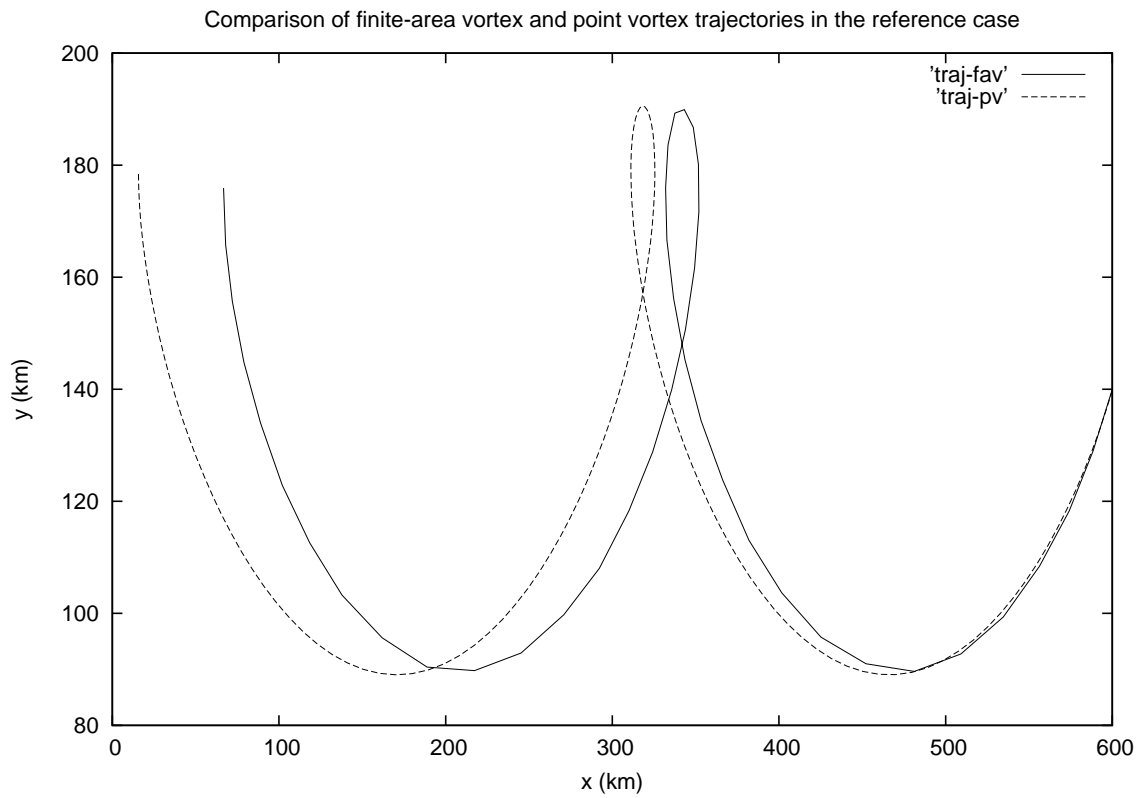


Figure 9: Comparison of the point vortex and finite area vortex trajectories in the upper layer, for the reference case (see also figure 3a); axes are graduated in km, using $R_d = 30$ km.

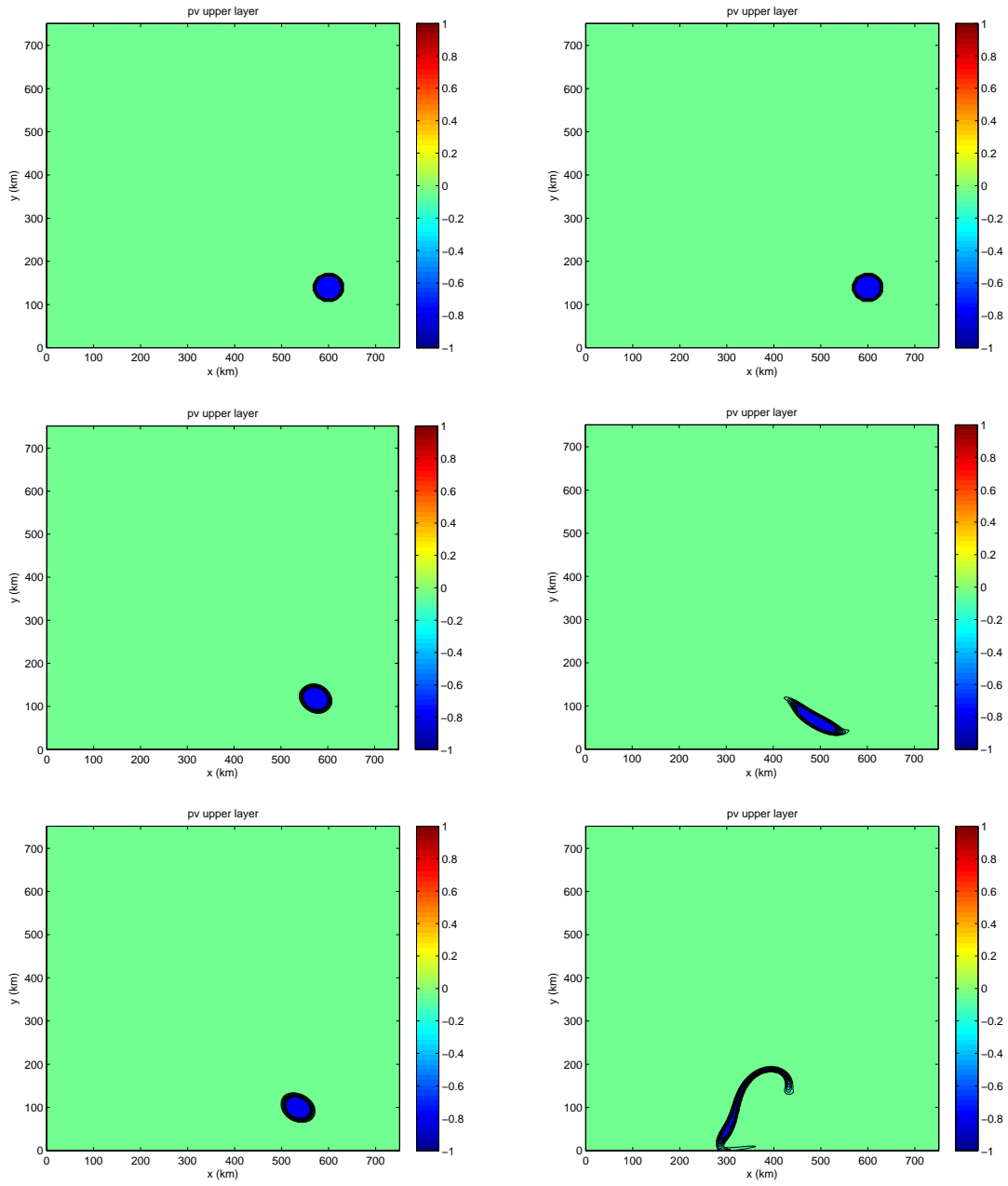


Figure 10: (top)

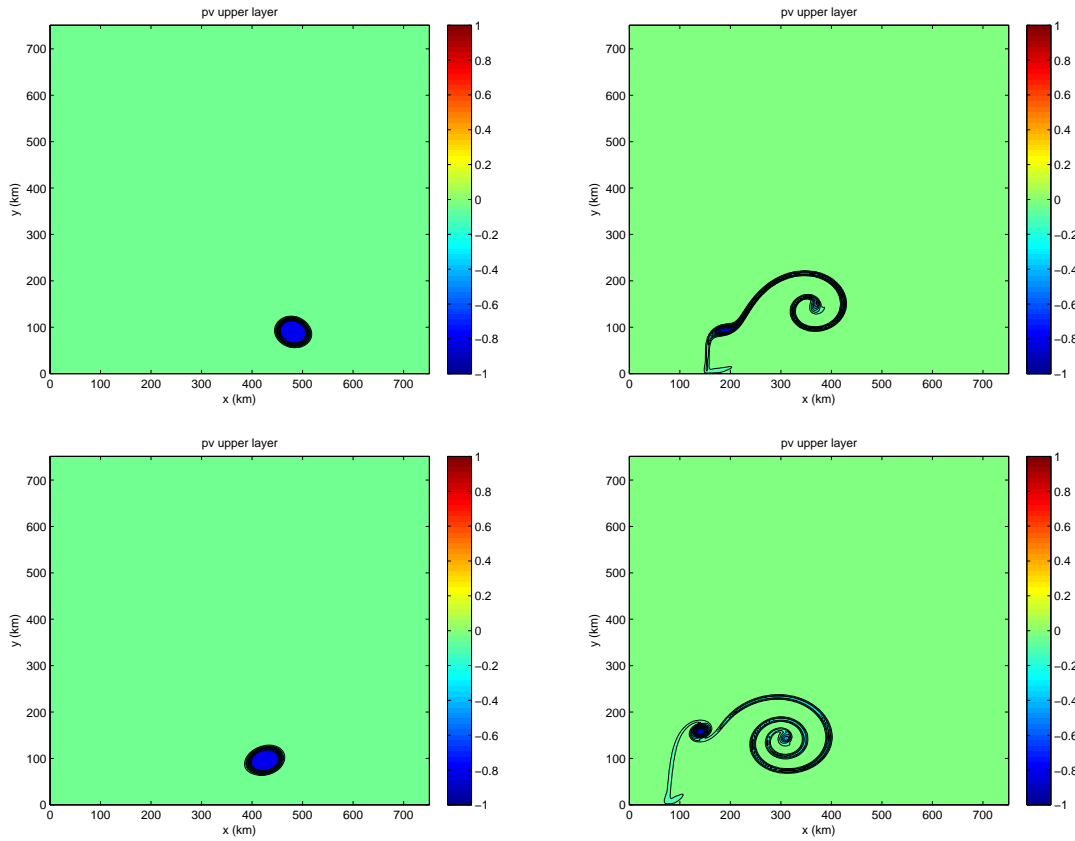


Figure 10: (bottom)

Time series of potential vorticity maps in the upper layer for the reference experiment (left column) and for another experiment with the same parameters except $Q_2/Q_1 = 4$ (right column). The reference experiment shows that the vortex shape remains little changed during its evolution, whereas in the other experiment, substantial filamentation (or partial splitting) occurs. Times (from top to bottom) are $t = 0, 20, 40, 60, 80$ days.

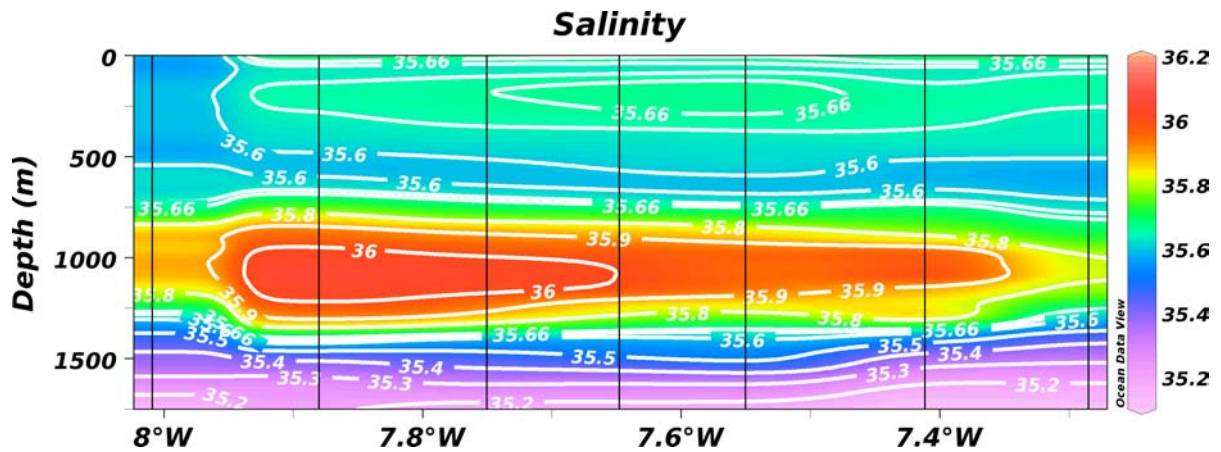


Figure 11: Zonal vertical salinity transect through the Meddy and the Swoddy cores. CTD measurements are from 2005/07/18 to 2005/07/19 (leg 2) at around $45^{\circ}03'N$. The westernmost point of measurement corresponds to a XCTD profile, obtained at the end of 2005/07/17.

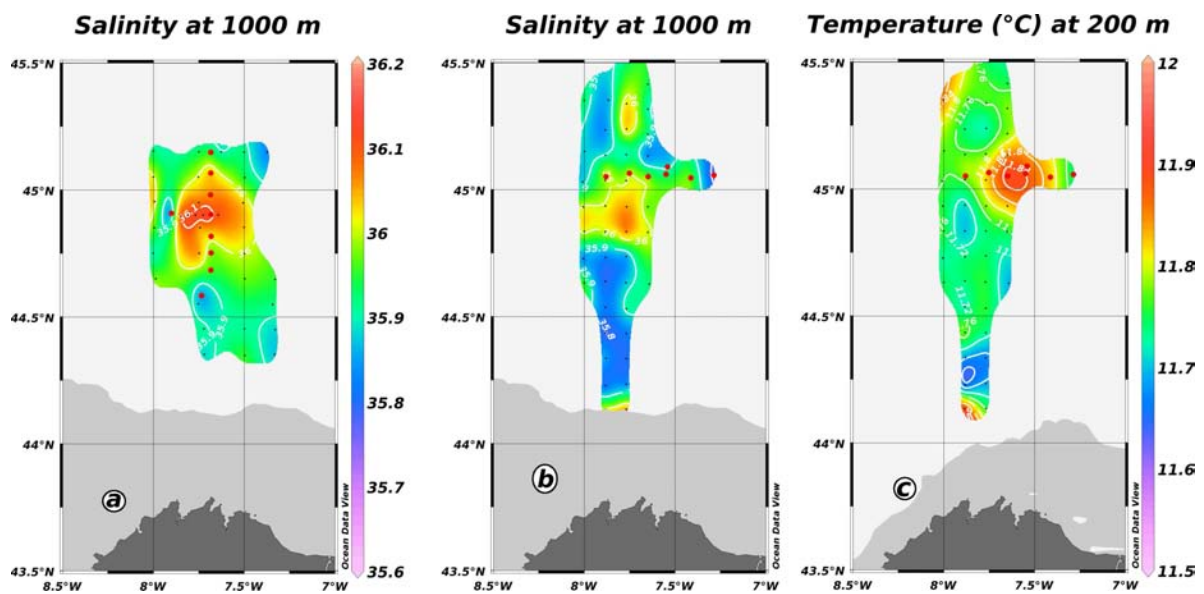


Figure 12: (a) Horizontal map of salinity at 1000 m obtained from CTD and XCTD measurements between 2005/07/01 and 2005/07/04 (leg 1). Grey contour is for the 1000 m isobath. (b) Horizontal map of salinity at 1000 m obtained from CTD and XCTD measurements between 2005/07/16 and 2005/07/19 (leg 2). Grey contour is the same as in (a). (c) Horizontal map of temperature at 200 m obtained from CTD and XCTD measurements between 2005/07/16 and 2005/07/19 (leg 2). Grey contour is for the 200 m isobath. Temperature map was preferred to salinity map, due to noise in XCTD data. Red dots indicate the position of CTD stations, while small black dots are for the XCTD measurements.

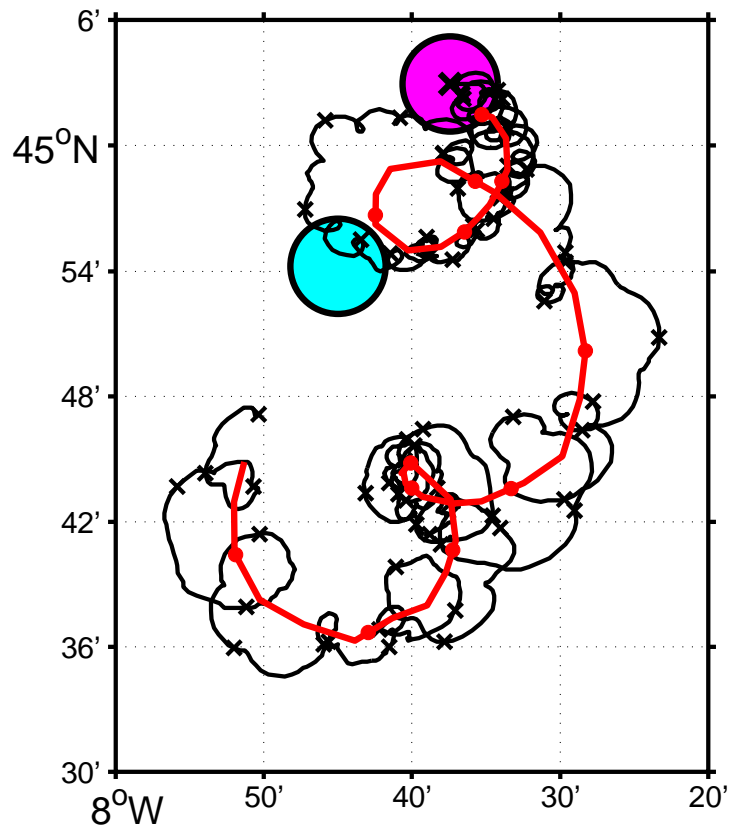


Figure 13: Black track: raw trajectory of buoy #30666 drogued at 200 m, deployed on 19/07/2005 (black cross at the center of large magenta spot). Black crosses along the black track are daily marks. The magenta (cyan) large dot circled in black indicate the position of the swoddy (meddy) core estimated from CTD/XCTD measurements at the beginning of the buoy track. The red track is the trajectory of the swoddy center, estimated from the buoy track (with red dots every 5 days).

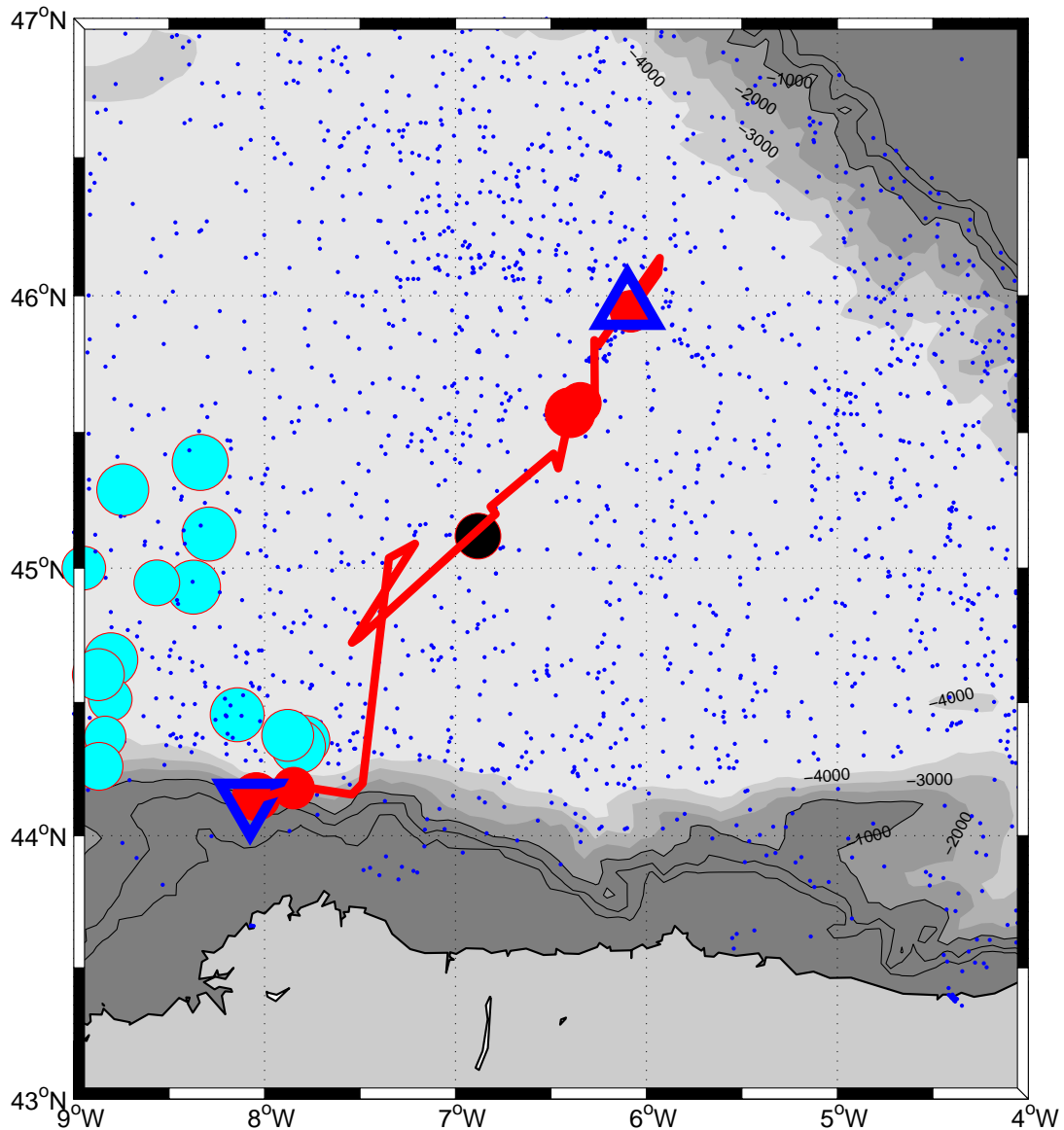


Figure 14: Map of salinity anomalies in the 700-1300 m range in the Bay of Biscay, derived from the analysis of ARGO floats up to May 2009 (see text). Positive salinity anomalies greater than 0.2 are plotted, as cyan, red and black dots. The area of the dots is proportional to strength of the anomaly. Salinity anomalies less than 0.2 are plotted, as blue points. Float # 4900557 anomaly # 1 (cycle 56, 2006/03/28) is plotted as a black dot. Float # 6900363 anomalies (anomaly # 2) are plotted as a red dots (from cycle 126, 2008/12/13, to cycle 137, 2009/04/02). Float # 6900363 underwater trajectory (between diving and surfacing points) is plotted as red solid 10 day segments. First diving point (2008/12/13) is indicated as a large downward pointing blue triangle and last surfacing position (2009/04/02) is indicated as a large upward pointing blue triangle.

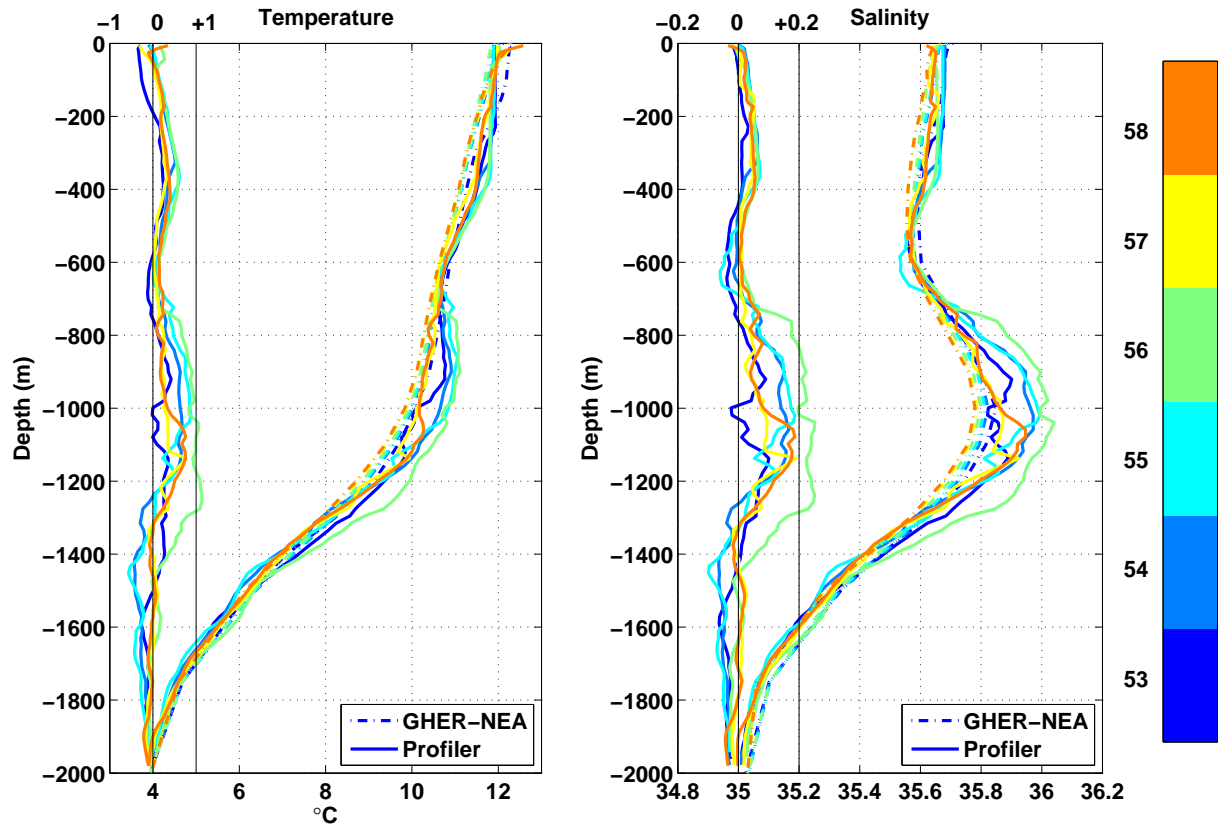


Figure 15: Individual vertical profiles for float # 4900557 (anomaly # 1, black dot in Figure 14). a) Temperature profiles as a function of depth. b) Salinity profiles as a function of depth. On each of the plots a and b: on the right of each figure, solid lines denote profiler data and dashed lines the monthly climatological profiles at the closest location (Troupin et al, 2010) with the scale at bottom of plot; on the left of each plot, are plotted the anomalies (profiler data minus monthly climatological data), with the scale at top of plot. Lines are color-coded as a function of cycle number (from cycle 53 (2006/02/26) to cycle 58 (2006/04/17)).

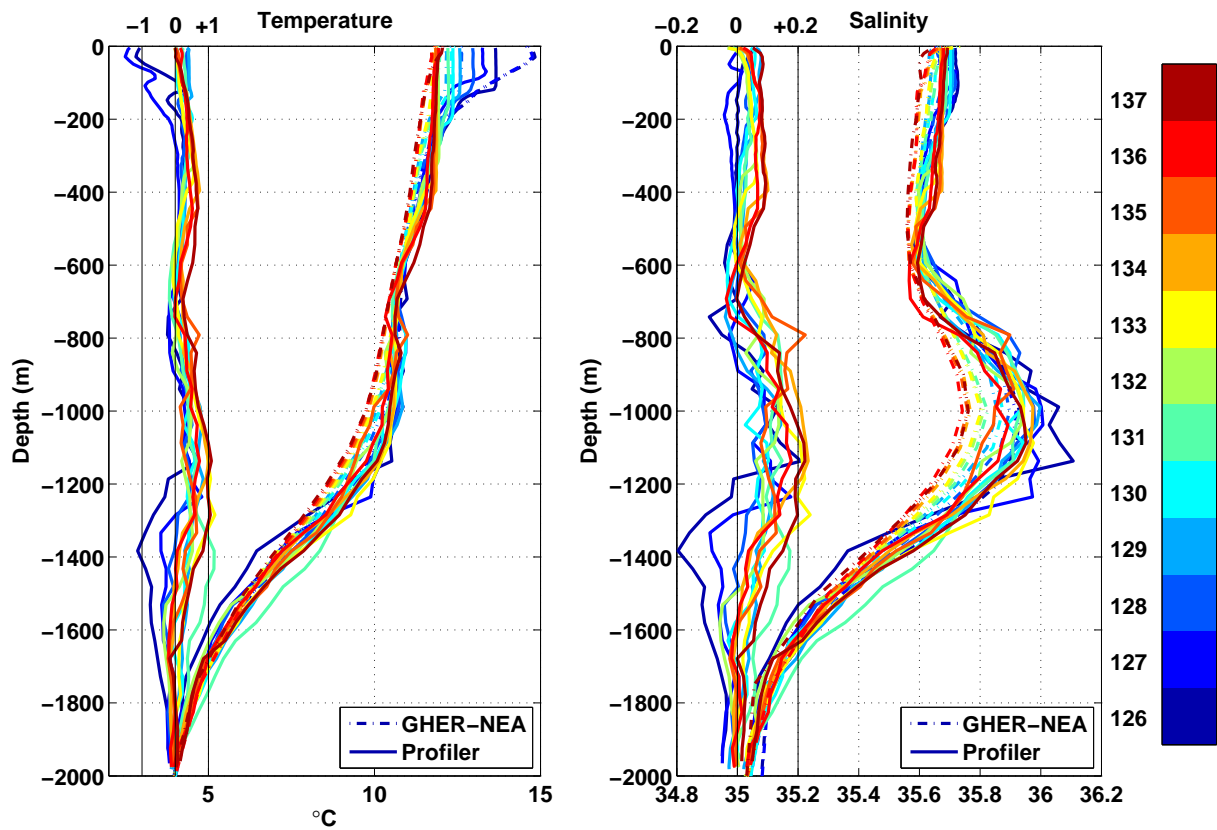


Figure 16: Same as for Figure 15 but for float # 6900363 (anomaly # 2, red dots and segments in Figure 14). Lines are color-coded as a function of cycle number (from cycle 126 (2008/12/13) to cycle 137 (2009/04/02)).